

# A Quantum Computing Implementation of Nuclear-Electronic Orbital (NEO) Theory: Towards an Exact pre-Born-Oppenheimer Formulation of Molecular Quantum Systems

Arseny Kovyrshin,<sup>1,\*</sup> Mårten Skogh,<sup>1,†</sup> Anders Broo,<sup>1,‡</sup> Stefano Mensa,<sup>2,§</sup> Emre Sahin,<sup>2,¶</sup> Jason Crain,<sup>3,4,\*\*</sup> and Ivano Tavernelli<sup>5,††</sup>

<sup>1</sup>*Data Science and Modelling, Pharmaceutical Sciences, R&D,*

*AstraZeneca Gothenburg, Pepparedsleden 1, Molndal SE-431 83, Sweden*

<sup>2</sup>*The Hartree Centre, STFC, Sci-Tech Daresbury, Warrington, WA4 4AD, United Kingdom*

<sup>3</sup>*IBM Research Europe, Hartree Centre STFC Laboratory,*

*Sci-Tech Daresbury, Warrington WA4 4AD, United Kingdom*

<sup>4</sup>*Department of Biochemistry, University of Oxford, Oxford, OX1 3QU, UK*

<sup>5</sup>*IBM Quantum, IBM Research Europe – Zurich, Säumerstrasse 4, 8803 Rüschlikon, Switzerland*

Nuclear quantum phenomena beyond the Born–Oppenheimer approximation are known to play an important role in a growing number of chemical and biological processes. While there exists no unique consensus on a rigorous and efficient implementation of coupled electron-nuclear quantum dynamics, it is recognised that these problems scale exponentially with system size on classical processors and therefore may benefit from quantum computing implementations. Here, we introduce a methodology for the efficient quantum treatment of the electron-nuclear problem on near-term quantum computers, based upon the Nuclear-Electronic Orbital (NEO) approach. We generalize the electronic two-qubit tapering scheme to include nuclei by exploiting symmetries inherent in the NEO framework; thereby reducing the hamiltonian dimension, number of qubits, gates, and measurements needed for calculations. We also develop parameter transfer and initialisation techniques, which improve convergence behavior relative to conventional initialisation. These techniques are applied to H<sub>2</sub> and malonaldehyde for which results agree with Nuclear-Electronic Orbital Full Configuration Interaction and Nuclear-Electronic Orbital Complete Active Space Configuration Interaction benchmarks for ground state energy to within 10<sup>-6</sup> Ha and entanglement entropy to within 10<sup>-4</sup>. These implementations therefore significantly reduce resource requirements for full quantum simulations of molecules on near-term quantum devices while maintaining high accuracy.

arXiv:2302.07814v1 [quant-ph] 15 Feb 2023

---

\* arseny.kovyrshin@astrazeneca.com

† marten.skogh@astrazeneca.com

‡ anders.broo@astrazeneca.com

§ stefano.mensa@stfc.ac.uk

¶ emre.sahin@stfc.ac.uk

\*\* jason.crain@ibm.com

†† ita@zurich.ibm.com

## I. INTRODUCTION

Chemical simulations at the atomic scale have advanced to the point where they are now capable of describing a wide range of phenomena including those occurring in complex systems and biological contexts. Much of this progress is due to advances in the power and efficiency of methods that can capture the quantum mechanical nature of electrons. Common to nearly all practical implementations of these techniques are two foundational simplifying assumptions: (a) that the atomic nuclei behave as classical particles and (b) that the Born–Oppenheimer (BO) approximation holds wherein the electrons are assumed to move sufficiently fast that they respond adiabatically to the nuclear motion [1].

It is however now widely acknowledged that, in systems containing light atoms, nuclear quantum effects are not negligible and can make appreciable contributions to processes including proton delocalization and tunneling, occurring *e.g.*, in biological systems [2] including enzymatic catalysis [3], in tautomeric transitions, and in determining the relative stability of crystal polymorphs [4]. The observation of an isotope-dependence in reaction rate [5] is a further particularly striking signature of nuclear quantum effects. Even in a familiar substance such as liquid and solid water, the presence of light atoms involved in hydrogen bonding [6] suggests that nuclear quantum effects can give important contributors to its static and dynamical properties [7, 8]. Finally, phenomena such as charge transfer reactions occurring for instance in photo-chemistry (*e.g.*, in the light harvesting complexes) may involve situations where the electronic potential energy surfaces (PES) become fully degenerate. At these so-called conical intersections, nuclear motion couples to more than a single PES and the adiabatic approximation breaks down opening new radiationless decay pathways. These examples provide a strong motivation for the extension of the current theoretical frameworks beyond the BO and classical nuclei approximations.

Currently, several methodologies have been developed that give a full quantum description of chemical systems. They are often referred to as the Nuclear-Electronic Orbital (NEO) approach [9], pre-Born–Oppenheimer (pBO) quantum theory [10], or Nuclear Orbital plus Molecular Orbital (NO+MO) theory [11]. In these formulations, nuclear tunneling and isotope effects arise naturally. Additionally, phenomena involving breakdown of the BO approximation are also captured. However, the computational cost of exact nuclear-electronic structure methods implemented on classical computers increases exponentially with the system size. In contrast, quantum processors have the potential to reduce this cost scaling to polynomial-time — underpinning the concept of quantum advantage [12–14].

Quantum computing is emerging as a new computational paradigm for the efficient solution of quantum mechanical problems, which can have a tremendous impact in different domains such as many-body physics [15–25], high energy physics [26–35], quantum chemistry [36–47], material design [48], biology and medicine [49–52]. The first quantum algorithm for treatment of both nuclei and electrons in a fully quantum simulation setting was proposed by Kassal *et al.* [53] and applied to the calculation of the quantum dynamics for the hydrogen molecule. Later, Veis *et al.* [54] adopted the NO+MO approach for constructing molecular Hamiltonians and proposed a QPE algorithm for computing the corresponding ground state wave function. Finally, Ollitrault *et al.* [55] presented a quantum algorithm for the simulation of nonadiabatic electron-nuclear dynamics including excited states.

The NEO approach is particularly versatile and stands as a compromise between the BO approximation and methodologies such as pBO. In the NEO approach, light mass nuclei are treated using orbital techniques in the same way as are the electrons. Furthermore, the BO separation between electronic and nuclear wave functions is — in general — not necessary in this case. On the contrary, the heavy nuclei (usually everything heavier than hydrogen) are described by classical point charges, determining the geometry of the molecular scaffold. Pavošević and Hammes-Schiffer [56] recently proposed a quantum computing implementation of the NEO approach employing the Variational Quantum Eigensolver (VQE) algorithm for the optimization of the hydrogen molecule and positronium hydride ground state wave functions, where only one proton was treated at quantum level.

In this study, we investigate the potential of the NEO approach for chemical systems and focus on the construction of the corresponding qubit Hamiltonian and wave function ansätze with the aim of accessing larger system sizes than have been previously investigated. Specifically, we explore and implement improved wave function parameterizations, operational mappings of second quantized molecular Hamiltonians to the qubit space, and efficient parameter initialization schemes for several electron-nuclear wave function ansätze. Particularly important are the devise of qubit tapering schemes such as two-qubit reduction, the exploitation of molecular point group symmetries, and the application of projectors to efficiently sample the relevant sectors of the molecular Fock space.

After a detailed description of the NEO Hamiltonian and of the corresponding wave function in the quantum computing setting, we tested our algorithm on the evaluation of the ground state energies of the hydrogen and malonaldehyde molecules using exact — noise-free — state vector VQE simulators. In the case of malonaldehyde, our approach was able to predict — despite the quite small size of the nuclear basis set and the imposed rigidity of the molecular scaffold — proton transfer barriers in reasonable good agreement with the available references. Exploiting the full quantum nature of the molecular wave function, we also proposed methods for the evaluation of additional interesting quantum features, such as the entanglement entropy of the subsystems (electronic and nuclear) from the full NEO wave function.

## II. THEORY

### A. Nuclear-Electronic Orbital Approach

Relative to the standard BO approximation, with point charges representing nuclei, the Hamiltonian in the NEO approach includes additional kinetic and potential energy operators for selected light nuclei. This approach incorporates the quantum effects of light nuclei and additionally introduces a separation between heavy and light nuclear motion. We denote the collective spatial coordinates of all quantum objects as  $\mathbf{r}$ , and additionally introduce superscripts where required to distinguish between nuclei,  $\mathbf{r}^n$ , and electrons,  $\mathbf{r}^e$ . We refer to both quantum nuclear and electronic coordinates combined as  $\mathbf{r} = \{\mathbf{r}^e, \mathbf{r}^n\}$ . The coordinates for classical nuclei will be denoted as  $\mathbf{R}$ . Quantities associated with electrons will carry lower case indices  $i, j$ , while upper case indices,  $I, J$ , are used for nuclear quantities, regardless of whether they are classical or not. The total wave function,  $\Psi(\mathbf{r}; \mathbf{R})$ , will still retain a parametric dependence on classical nuclear coordinates,  $\mathbf{R}$ . Thus the Schrödinger equation reads as follows (in atomic units)

$$\left[ -\sum_i^{N^e} \frac{1}{2} \nabla_i^2 - \sum_I^{N^n} \frac{1}{2M_I} \nabla_I^2 - \sum_{i,I}^{N^e, N^n} \frac{Z_I}{|\mathbf{r}_i - \mathbf{r}_I|} + \sum_{i<j}^{N^e} \frac{1}{|\mathbf{r}_i - \mathbf{r}_j|} - \sum_{i,A}^{N^e, N^c} \frac{Z_A}{|\mathbf{r}_i - \mathbf{R}_A|} + \sum_{I,A}^{N^n, N^c} \frac{Z_I Z_A}{|\mathbf{r}_I - \mathbf{R}_A|} + \sum_{A<B}^{N^c} \frac{Z_A Z_B}{|\mathbf{R}_A - \mathbf{R}_B|} \right] \Psi(\mathbf{r}; \mathbf{R}) = E \Psi(\mathbf{r}; \mathbf{R}), \quad (1)$$

where  $Z_I$  are nuclear charges,  $M_I$  nuclear masses,  $N^e$ ,  $N^n$ , and  $N^c$  are the total number of electrons, quantum nuclei, and classical nuclei, respectively.

The NEO approach solves Eq. (1) using both electronic,

$$\phi_i(\mathbf{x}_i) \equiv \phi_i(\mathbf{r}_i, s_i), \quad (2)$$

and nuclear,

$$\phi_I(\mathbf{x}_I) \equiv \phi_I(\mathbf{r}_I, s_I), \quad (3)$$

spin orbitals constructed separately from nuclear and electronic basis sets, originally in Gaussian basis sets [9]. Note that the spin coordinates  $s_i$  in Eqs. (2,3) are combined together with  $\mathbf{r}_i$  into a new variable  $\mathbf{x}_i$  for brevity. Based on these spin orbitals one can form antisymmetric products, Slater determinants, for electrons

$$\Phi_\mu(\mathbf{x}^e) = \hat{S}^- \prod_i \phi_i(\mathbf{x}_i^e), \quad (4)$$

and symmetric or antisymmetric spin orbital products for bosonic or fermionic nuclei, correspondingly,

$$\Phi_\nu(\mathbf{x}^n) = \hat{S}^\pm \prod_I \phi_I(\mathbf{x}_I^n), \quad (5)$$

where  $\hat{S}^{+/-}$  are symmetrizer/antisymmetrizer operators. These constitute the multi-particle basis set for the Nuclear-Electronic Orbital Full Configuration Interaction (NEOFICI) approach [9], which expresses the nuclear-electronic wave function as follows

$$\Psi(\mathbf{x}; \mathbf{R}) = \sum_{\mu\nu}^{C^e, C^n} C_{\mu\nu} \Phi_\mu(\mathbf{x}^e) \Phi_\nu(\mathbf{x}^n), \quad (6)$$

where  $C^e$  and  $C^n$  are the total number of electronic and nuclear states, Eq. (4) and (5). We emphasize that in Eq. (6) only one type of nuclei is considered. In the most general case, each type of nuclei will have its own set of spin orbitals and corresponding symmetric or antisymmetric product, which in turn enters the sum in Eq. (6). As in this work, we will only consider protons and electrons as quantum particles, only masses  $M_I = M = 1874 m_e$  and charges  $Z_I = 1 e$  will be considered in the quantum part of the Hamiltonian. Within such a framework, one gets the following second

quantization representation for the Hamiltonian [9]

$$\begin{aligned}
\hat{H} = & - \sum_{ij} \left[ \int \phi_i^*(\mathbf{x}) \frac{1}{2} \nabla^2 \phi_j(\mathbf{x}) d\mathbf{x} \right] \hat{a}_i^\dagger \hat{a}_j - \sum_{IJ} \left[ \int \phi_I^*(\mathbf{x}) \frac{1}{2M} \nabla^2 \phi_J(\mathbf{x}) d\mathbf{x} \right] \hat{a}_I^\dagger \hat{a}_J \\
& + \frac{1}{2} \sum_{ijkl} \left[ \int \phi_i^*(\mathbf{x}_1) \phi_k^*(\mathbf{x}_2) \frac{1}{|\mathbf{r}_1 - \mathbf{r}_2|} \phi_l(\mathbf{x}_2) \phi_j(\mathbf{x}_1) d\mathbf{x}_1 d\mathbf{x}_2 \right] \hat{a}_i^\dagger \hat{a}_k^\dagger \hat{a}_l \hat{a}_j \\
& + \frac{1}{2} \sum_{IJKL} \left[ \int \psi_I^*(\mathbf{x}_1) \psi_K^*(\mathbf{x}_2) \frac{1}{|\mathbf{r}_1 - \mathbf{r}_2|} \psi_L(\mathbf{x}_2) \psi_J(\mathbf{x}_1) d\mathbf{x}_1 d\mathbf{x}_2 \right] \hat{a}_I^\dagger \hat{a}_K^\dagger \hat{a}_L \hat{a}_J \\
& - \sum_{ijKL} \left[ \int \phi_i^*(\mathbf{x}_1) \psi_K^*(\mathbf{x}_2) \frac{1}{|\mathbf{r}_1 - \mathbf{r}_2|} \psi_L(\mathbf{x}_2) \phi_j(\mathbf{x}_1) d\mathbf{x}_1 d\mathbf{x}_2 \right] \hat{a}_i^\dagger \hat{a}_K^\dagger \hat{a}_L \hat{a}_j \\
& + \sum_{IJ,A} \left[ \int \phi_I^*(\mathbf{x}) \frac{Z_A}{|\mathbf{r} - \mathbf{R}_A|} \phi_J(\mathbf{x}) d\mathbf{x} \right] \hat{a}_I^\dagger \hat{a}_J - \sum_{ij,A} \left[ \int \phi_i^*(\mathbf{x}) \frac{Z_A}{|\mathbf{r} - \mathbf{R}_A|} \phi_j(\mathbf{x}) d\mathbf{x} \right] \hat{a}_i^\dagger \hat{a}_j \\
& + \frac{1}{2} \sum_{AB} \frac{Z_A Z_B}{|\mathbf{R}_A - \mathbf{R}_B|}. \quad (7)
\end{aligned}$$

Note that in addition to anti-commutation relations between indistinguishable fermions

$$[\hat{a}_i^\dagger, \hat{a}_j]^+ = \delta_{ij} \quad (8)$$

$$[\hat{a}_i^\dagger, \hat{a}_j^\dagger]^+ = [\hat{a}_i, \hat{a}_j]^+ = 0 \quad (9)$$

$$[\hat{a}_I^\dagger, \hat{a}_J]^+ = \delta_{IJ} \quad (10)$$

$$[\hat{a}_I^\dagger, \hat{a}_J^\dagger]^+ = [\hat{a}_I, \hat{a}_J]^+ = 0 \quad (11)$$

distinguishable fermions do commute (between protons and electrons), implying

$$[\hat{a}_I^\dagger, \hat{a}_j] = 0 \quad (12)$$

$$[\hat{a}_I^\dagger, \hat{a}_j^\dagger] = [\hat{a}_I, \hat{a}_j] = 0. \quad (13)$$

If bosonic nuclei are considered then the following commutation relations hold for indistinguishable particles

$$[\hat{a}_I^\dagger, \hat{a}_J] = \delta_{IJ}, \quad (14)$$

$$[\hat{a}_I^\dagger, \hat{a}_J^\dagger] = [\hat{a}_I, \hat{a}_J] = 0 \quad (15)$$

and the same relation as above, Eqs. (12,13), between the distinguishable particles.

## B. Quantum Computing Ansatz

The VQE is a quantum variational algorithm that uses a classical optimization routine to find the parameters of a quantum state that minimizes the expectation value of a given molecular Hamiltonian [57]. Some of the key advantages of the VQE algorithm include its ability to be implemented on near-term quantum computers which have a limited number of qubits and are prone to errors, and its potential to scale to larger systems, hence becoming a tool for practical applications in the near future [58–61].

Mathematically, the VQE optimization algorithm can be expressed as follows. Let  $\hat{H}$  be the Hamiltonian of the system and let  $|\psi(\boldsymbol{\theta})\rangle$  be the trial state, which is a function of parameters  $\boldsymbol{\theta}$ . The goal is to find the values of  $\boldsymbol{\theta}$  that minimize the expectation value of the Hamiltonian, given by

$$E(\boldsymbol{\theta}) = \langle \psi(\boldsymbol{\theta}) | \hat{H} | \psi(\boldsymbol{\theta}) \rangle. \quad (16)$$

To find the optimal values of  $\theta$ , we can use a classical optimization algorithm to iteratively update the values of  $\theta$ . Then, the quantum part of the algorithm is used to apply the quantum circuit to the quantum state of the system and measure the energy of the resulting state until the minimum value of  $E(\theta)$  is found.

For the VQE optimization of the system wave function within a quantum computing setting, it is desirable to design a flexible, expressive and well-behaved ansatz, which can deliver good accuracy with the fewest number of parameters. While there are a vast number of different ansätze available, in this work we focus on the Unitary Coupled Cluster and hardware-efficient parameterizations. The main advantage of the latter arises from the shallow circuit depth required for its implementation — an important prerequisite for near-term (non-fault tolerant) hardware [62]. Unfortunately, for chemical systems, there is no systematic, practical approach for the initialization and optimization of the variational parameters when using hardware-efficient ansätze. Moreover, these often show limited expressivity while the optimization process suffers from the presence of barren plateaus [63]. Here we will explore several variants of the TwoLocal hardware-efficient ansatz [64] for the NEO wave function; details of which will be discussed in Section IV B.

In contrast to hardware-efficient ansätze, the Unitary Coupled Cluster (UCC) ansatz has a very well-tailored parameter space and naturally approximates wave functions for chemical systems. This well-established quantum chemistry ansatz was first introduced for VQE by Peruzzo *et al.* [57]. Although the resulting quantum circuits are in general deeper than the hardware-efficient ones, the optimization of the UCC circuit is less prone to barren plateaus, and lack of particle, total spin, and spin projection conservation. This becomes especially important when one uses multiple centers for protons and electrons, leading hardware-efficient ansatz optimizations to the wrong results with an incorrect number of electrons and nuclei.

While a hardware-efficient ansatz does not require any special adaptation for the NEO wave function, we must introduce tailored modifications to the UCC ansatz to extend it from the purely electronic to the NEO case. Here we refer to the modified forms as NEOUCC. The parameterized unitary operators  $\hat{U}_{CC}(\mathbf{t})$ ,

$$\hat{U}_{CC}(\mathbf{t}) = e^{\hat{T}(\mathbf{t}) - \hat{T}^\dagger(\mathbf{t})} \quad (17)$$

are at the core of the UCC ansatz. Acting upon some initial state  $|\psi_{init}\rangle$  (typically the Hartree-Fock solution) it produces a trial wave function of the form

$$|\psi(\mathbf{t})\rangle = \hat{U}_{CC}(\mathbf{t}) |\psi_{init}\rangle. \quad (18)$$

In general, the operator  $\hat{T}$  is given as a sum of cluster operators of increasing order, *i.e.*, the number of particles being acted on,  $o$ ,

$$\hat{T} = \sum_o \hat{T}^{(o)} = \hat{T}^{(1)} + \hat{T}^{(2)} + \dots \quad (19)$$

In other words,  $o = 1$  corresponds to one-particle excitations,  $o = 2$  to two-particle excitations, and so on. In second quantization these are expressed as

$$\hat{T}^{(1)} = \sum_{pq} t_q^p \hat{a}_p^\dagger \hat{a}_q \quad (20)$$

$$\hat{T}^{(2)} = \sum_{pqrs} t_{rs}^{pq} \hat{a}_p^\dagger \hat{a}_r \hat{a}_q^\dagger \hat{a}_s. \quad (21)$$

Here  $p, q, r, s$  index all spin orbitals, both protonic and electronic, and  $t$  represents coefficients to be optimized. Labeling the initially occupied spin orbitals with  $i, j, k, l$  and the initially unoccupied spin orbitals with  $a, b, c, d$  (analogous for protons using upper case:  $I, J, K, L$  and  $A, B, C, D$ ) we can limit the cluster operators to a subset that conforms to chosen occupations of the initial state

$$t_{ij\dots IJ\dots}^{ab\dots AB\dots} \prod_{\gamma,\lambda} \hat{a}_\gamma^\dagger \hat{a}_\lambda \prod_{\Gamma,\Lambda} \hat{a}_\Gamma^\dagger \hat{a}_\Lambda, \quad (22)$$

where  $\gamma \subseteq \{a, b, \dots\}$ ,  $\lambda \subseteq \{i, j, \dots\}$ ,  $\Gamma \subseteq \{A, B, \dots\}$ ,  $\Lambda \subseteq \{I, J, \dots\}$ . That is, annihilation (creation) operators will only act on occupied (unoccupied) spin orbitals, indexed as  $a, b, c, d, \dots$  ( $i, j, k, l, \dots$ ) for electronic spin orbitals and as  $A, B, C, D, \dots$  ( $I, J, K, L, \dots$ ) for protonic spin orbitals. Since we now obtain a mix of electron and proton operators we introduce a dual superscript  $\hat{T}^{(e,p)}$  where the first index,  $e$ , is the order of electronic excitation in each operator, and  $p$  is similarly the order of the protonic excitations, that is

$$\hat{T} = \sum_{e,p} \hat{T}^{(e,p)}, \quad (23)$$

where  $\hat{T}^{(e,p)}$  is *e.g.*

$$\hat{T}^{(1,0)} = \sum_{ia} t_i^a \hat{a}_a^\dagger \hat{a}_i \quad (24)$$

$$\hat{T}^{(0,1)} = \sum_{IA} t_I^A \hat{a}_A^\dagger \hat{a}_I \quad (25)$$

$$\hat{T}^{(2,0)} = \sum_{ijab} t_{ij}^{ab} \hat{a}_a^\dagger \hat{a}_i \hat{a}_b^\dagger \hat{a}_j \quad (26)$$

$$\hat{T}^{(0,2)} = \sum_{IJAB} t_{IJ}^{AB} \hat{a}_A^\dagger \hat{a}_I \hat{a}_B^\dagger \hat{a}_J \quad (27)$$

$$\hat{T}^{(1,1)} = \sum_{iJaB} t_{iJ}^{aB} \hat{a}_a^\dagger \hat{a}_i \hat{a}_B^\dagger \hat{a}_J \quad (28)$$

The sum in Eq. (23) is normally truncated to some fixed order of  $e$  and  $p$ . Electronic structure VQE calculations are often limited to one- and two-particle cluster operators, while higher orders are ignored. This approximation is commonly referred to as Unitary Coupled Cluster Singles and Doubles (UCCSD). We will extend this notation to indicate when different orders are used for electrons, protons and mixed terms, respectively. For example, an ansatz using singles and doubles for electrons and nuclei, while using a mixed double consisting of single electronic and single nuclear excitations, a mixed triple consisting of double electronic, and single nuclei operators will be indicated as

$$\text{UCCSDT}^{(2,1)} \Rightarrow \overbrace{\hat{T}^{(1,0)} + \hat{T}^{(0,1)}}^{\text{S}} + \underbrace{\hat{T}^{(2,0)} + \hat{T}^{(1,1)} + \hat{T}^{(0,2)}}_{\text{D}} + \hat{T}^{(2,1)}. \quad (29)$$

Note that the lack of superscript implies use of all  $o$ -particle operators, *i.e.*,  $\text{S} \Rightarrow \hat{T}^{(1,0)} + \hat{T}^{(0,1)}$ ,  $\text{D} \Rightarrow \hat{T}^{(2,0)} + \hat{T}^{(1,1)} + \hat{T}^{(0,2)}$ ,  $\text{T} \Rightarrow \hat{T}^{(3,0)} + \hat{T}^{(2,1)} + \hat{T}^{(1,2)} + \hat{T}^{(0,3)}$ , *etc.* For systems with fewer electrons or protons than the excitation order,  $n_e < e + p$  or  $n_n < e + p$ , only mixed operators are considered. For example, in the case of the hydrogen molecule, the possible triple and quadruple excitation operators are  $\text{T} \Rightarrow \hat{T}^{(2,1)} + \hat{T}^{(1,2)}$  and  $\text{Q} \Rightarrow \hat{T}^{(2,2)}$ , respectively.

### C. Ansatz Initialization

The initial guess for parameters in any variational quantum algorithm is in many cases important to the performance of the calculation and can be crucial. Having a proper initial guess can reduce the number of evaluations needed to reach convergence, while also allowing convergence to the correct minimum (or maximum). As such, it proves wise to choose initial values for the ansatz parameters with care. For hardware-efficient ansätze this is especially vital, where otherwise initial parameters often are chosen randomly, making convergence to a global minimum difficult.

The convergence problem arises due to several factors, *e.g.*, the presence of local minima in the optimization landscape, and the presence of barren plateaus [63, 65]. As these problems compound with the number of variational parameters, it can be useful to solve an approximate problem in order to find a set of starting parameters closer to those of the true ground state. In the case of NEO calculations, one such approximate solution can be taken from the conventional electronic structure calculations under the BO approximation and with nuclei represented as classical point charges. Thus we suggest initializing the parameters for the electronic part of the NEO calculation with those from the converged electronic structure calculation. For the case of NEOUCC ansatz, the circuit operators corresponding to electronic, nuclear, and mixed excitations can be separated according to Figure 1. As  $U_{T^{(e,0)}}(\boldsymbol{\theta}^e)$  operators are the same for NEO and electronic cases one can initialize their parameters,  $\boldsymbol{\theta}^e$ , with those from the electronic calculation and set all other parameters to zero,  $\boldsymbol{\theta}^{0,n} = \boldsymbol{\theta}^{e,n} = \mathbf{0}$ .

For a hardware-efficient ansatz, the parameter transfer becomes slightly more complicated as it is difficult to assign given parameters to specific nuclear or electronic parts. Therefore, special care should be taken such that the parameter transfer only affects qubits associated with electronic orbitals. A generalized construction of the TwoLocal ansatz can be created from sets of parameterized single qubit rotational gates separated by entangling gates applied between qubits. Both the electronic and NEO problems can be represented in this manner, see Figure 2. In general, the number of layers needed to accurately describe the electronic problem,  $d_{\text{EL}}$ , is smaller or equal to  $d_{\text{NEO}}$ , the number of layers needed to describe the NEO problem. With this in mind and a proper selection of entangling scheme, one can find a transfer protocol between electronic and NEO parameters. In Section IV B we present in detail the two variants of parameter initialization employing CZ entangling layers. CZ entangling layers are beneficial in that they

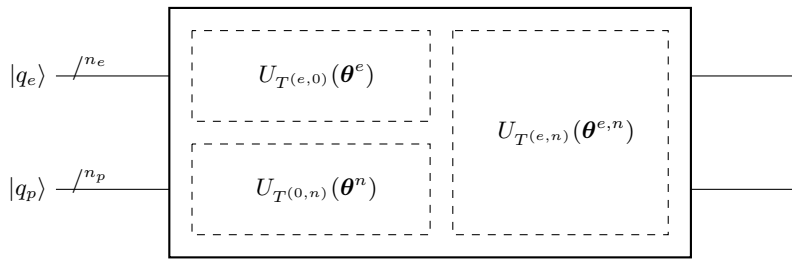


Figure 1: Schematic circuit used for the initialization of the electronic parameters of NEOUCC ansatz. The conventional electronic operators can be considered as a subset of the NEO operators.  $n_e$  and  $n_p$  are the numbers of qubits representing electron and proton spin orbitals, respectively.

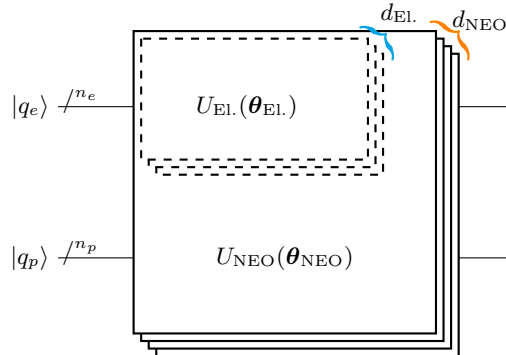


Figure 2: Schematic circuit used for the initialization of the electronic parameters in the NEO hardware-efficient ansatz. The electronic and NEO hardware-efficient circuits have  $d_{\text{EI.}}$  and  $d_{\text{NEO}}$  layers, respectively.  $n_e$  and  $n_p$  are the numbers of qubits representing electron and proton spin orbitals.

allow for the limited influence of electronic parameters on nuclear qubits if the nuclear parameters are unset (equal to zero).

The suggested initialization schemes assumes that the electronic parameters could also be relaxed during the wave function optimization. It would be especially important for cases where multiple BO potential energy surfaces intersect. Also, one should assure that the presence of additional nuclear orbitals in the NEO representation preserves the point group symmetry of the system. Nonetheless, even if the point group symmetry is the same, the corresponding  $\mathbb{Z}_2$ -symmetry reduction might introduce a difference in the sign pattern between the off-diagonal elements of the NEO and electronic qubit Hamiltonians. This stems from the difference in sign between eigenvalues of  $\mathbb{Z}_2$ -symmetry for the NEO and electronic states and must be taken into account during the parameter transfer. We describe the procedure in detail in Section IV B.

#### D. Entanglement Entropy Measurement

The measurement of the entanglement entropy (or von Neumann entropy) can provide additional insights into the correlation between the two particle subsystems, namely electrons and nuclei. This is particularly interesting when studying systems composed of distinguishable particles and will provide a direct measurement of the entanglement between the two subsystems. Here we will introduce the subsystem entropy in the NEO framework as

$$s_i = -\text{Tr}(\hat{\rho}^i \ln \hat{\rho}^i), \quad (30)$$

where  $i \in \{e, n\}$ ,  $\hat{\rho}^e = \text{Tr}_n \hat{\rho}^{e,n}$  and  $\hat{\rho}^n = \text{Tr}_e \hat{\rho}^{e,n}$  are the corresponding reduced density matrices, and  $\hat{\rho}^{e,n}$  is the full density matrix.

### III. COMPUTATIONAL DETAILS

The NEO framework was implemented in a locally modified version of Qiskit [64]. All quantum computing calculations were performed as state vector simulations using variations of the TwoLocal ansatz as well as NEOUCC ansätze. The former employed parameterized  $R_y$  and  $R_z$  single rotation gates together with CZ entangling gates. The various entanglement patterns used in this work are summarized in Sections IV B and IV C. All the classical algorithm calculations were carried out using the GAMESS-US software package [66]. In order to prepare the test systems and reference results the Nuclear Electronic Orbitals Hartree–Fock (NEOHF), NEOFCI, and Nuclear-Electronic Orbital Complete Active Space Configuration Interaction (NEOCASCI) [9] calculations were performed. The system Hamiltonians were expanded in the orbitals obtained from the NEOHF calculations, and the corresponding NEO wave functions were optimized with the VQE algorithm in Qiskit. The SciPy [67] implementations of the Constrained Optimization By Linear Approximation (COBYLA) [68], Conjugate Gradient (CG) [69, 70], and Sequential Least Squares Programming (SLSQP) [71] methods were used for the optimization of the circuit parameters. The fermion-to-qubit transformation used to map the electronic and nuclear operators together with the employed qubit reduction techniques are described in Section III A. The additional qubit space reduction obtained by exploiting the NEO Hamiltonian’s point group symmetries are discussed in Section (III B).

#### A. Fermionic Mapping and 4-qubit Reduction

The fermionic parity mapping [60] scheme is used in this work for both electronic and nuclear second-quantized operators. Note that we are only treating nuclei consisting of single protons quantum mechanically, and as such, only fermionic representations are necessary. We assume that the fermionic occupation number basis vectors are written in what we will refer to as particle-spin block representation

$$|f\rangle = \underbrace{|f_{n_\beta^p+n_\alpha^p}^p, \dots, f_{1+n_\alpha^p}^p\rangle}_{\beta\text{-spin prot.}} \underbrace{|f_{n_\alpha^p}^p, \dots, f_1^p\rangle}_{\alpha\text{-spin prot.}} \underbrace{|f_{n_\beta^e+n_\alpha^e}^e, \dots, f_{1+n_\alpha^e}^e\rangle}_{\beta\text{-spin elec.}} \underbrace{|f_{n_\alpha^e}^e, \dots, f_1^e\rangle}_{\alpha\text{-spin elec.}}, \quad f_i^{e/p} \in \{0, 1\}, \quad (31)$$

where  $f_i^e$  and  $f_i^p$  are the spin orbital occupation numbers for electrons and protons respectively, and  $n_\alpha^e, n_\beta^e, n_\alpha^p, n_\beta^p$  are the number of  $\alpha$  and  $\beta$  spin orbitals for the two types of particle. With parity encoding, instead of storing the occupation of individual spin orbitals, the qubits store information about the parity of the fermionic state as follows

$$p_i^{e/p} = \bigoplus_{j=1}^i f_j^{e/p}, \quad (32)$$

where  $\bigoplus$  represents addition modulo 2. A change to the parity encoding thus yields the parity state

$$|p\rangle = \underbrace{|p_{n_\beta^p+n_\alpha^p}^p, \dots, p_{1+n_\alpha^p}^p\rangle}_{\beta\text{-spin prot.}} \underbrace{|p_{n_\alpha^p}^p, \dots, p_1^p\rangle}_{\alpha\text{-spin prot.}} \underbrace{|p_{n_\beta^e+n_\alpha^e}^e, \dots, p_{1+n_\alpha^e}^e\rangle}_{\beta\text{-spin elec.}} \underbrace{|p_{n_\alpha^e}^e, \dots, p_1^e\rangle}_{\alpha\text{-spin elec.}}, \quad p_i^{e/p} \in \{0, 1\}, \quad (33)$$

thus mapping the local state of each spin orbital to the state of several qubits. Note, that the qubit mapping for each type of particle is performed within the corresponding subspace, such that the parity of electronic qubits is not affected by the state of nuclear qubits, and vice versa.

The fermionic creation and annihilation operators in the parity basis have the following representations

$$a_i^\dagger \equiv \frac{1}{2} [X_{i+1}^\leftarrow \otimes (X_i \otimes Z_{i-1} - iY_i)], \quad (34)$$

$$a_i \equiv \frac{1}{2} [X_{i+1}^\leftarrow \otimes (X_i \otimes Z_{i-1} + iY_i)]. \quad (35)$$

Here we introduce  $X_{i+1}^\leftarrow$  as an operator that acts on all qubits of index  $i+1$  and higher within the electronic or nuclear subspaces, accounting for fermionic antisymmetry under the exchange of identical particles. For the edge case of  $i=1$ , the expression simplifies to  $\frac{1}{2} [X_{i+1}^\leftarrow \otimes (X_i + iY_i)]$ , and similarly for  $i = n_\alpha^{e/p} + n_\beta^{e/p}$  we get  $\frac{1}{2} (X_i \otimes Z_{i-1} + iY_i)$ .

The utilization of the parity encoding simplifies the identification of the discrete  $\mathbb{Z}_2$ -symmetries associated with the particle number operators within the  $\alpha$  and  $\beta$  subspaces [72] for both electrons and nuclei. As we are dealing with

a Hamiltonian based on the non-relativistic Schrödinger equation, Eq. (1), the number of particles within the  $\alpha$  and  $\beta$  subspaces are conserved and therefore total parity numbers such as  $p_{n_{\beta}^p+n_{\alpha}^p}$ ,  $p_{n_{\alpha}^p}$ ,  $p_{n_{\beta}^e+n_{\alpha}^e}$ , and  $p_{n_{\alpha}^e}$  are constant. The corresponding 4 qubits can thus be treated classically and their contribution to the expectation value of the Hamiltonian can be calculated beforehand employing the “tapering” procedure described in Ref. [72].

## B. Qubit Reduction from Hamiltonian Symmetries

If a molecular system obeys some point group symmetry, the number of qubits can be further reduced using methods introduced by Bravyi *et al.* [72]. This approach allows for additional qubit tapering by identifying a  $\mathbb{Z}_2$ -symmetry of the Hamiltonian corresponding to the specific molecular point group symmetry.

In addition, when the system wave function can be restricted to specific subspaces of the total Hilbert space, one can further impose an additional  $\mathbb{Z}_2$ -symmetry, which confines the solutions in the region of interest. This may, for example, happen in the case of the hydrogen molecule if one is interested in the orthohydrogen nuclear isomer, the dominant nuclear spin isomer (75%) at room temperature. Thus one can just consider the maximally spin-polarized triplet state for the protons. This allows for either alpha or beta spin orbitals to be ignored. To reduce our active space to the selected set of nuclear alpha or beta orbitals, we introduce (here for the case of orthohydrogen) a projector to states for which beta spin orbitals are unoccupied

$$\hat{P} = \bigotimes_J^{\beta \text{ nuc.}} \frac{1}{2}(I + Z) \bigotimes_I^{\alpha \text{ nuc.}} I \bigotimes_i^{\text{elec.}} I \quad (36)$$

and produce the projected Hamiltonian

$$\hat{H}_P = \hat{P}\hat{H}\hat{P}. \quad (37)$$

In this case, one can find as many  $\mathbb{Z}_2$ -symmetries as the number of beta spin orbitals and the qubits corresponding to these spin orbitals can be therefore tapered off. This operation can also be performed in the Hamiltonian construction procedure by simply removing terms containing creation/annihilation operators acting on these spin orbitals.

## IV. RESULTS

Our simulations focused on the evaluation of the NEO ground state energies and entanglement entropies for  $\text{H}_2$  and malonaldehyde. We first introduce a detailed description of the two systems and describe the conditions under which the conventional quantum chemistry calculations were performed. We then describe (in Section IV B) the procedures for the initialization of the quantum computing calculations, as well as the transformations employed in the mapping of the fermionic electronic structure problem in the qubit space (see Sections III A and III B). In Section IV C, we will report the results for the hydrogen molecule, discussing the performance of the different wavefunction ansätze, including the one inspired by UCC and the more quantum native, hardware efficient, TwoLocal ansatz. Finally, in Section IV D we will present and discuss the results for the second and more challenging system, malonaldehyde, which is a prototypical system used to investigate quantum effects in molecular proton transfer reactions. In this case, the delocalization of the proton wave function between the donor and acceptor moieties makes the choice of the proton basis set and wave function ansatz more challenging than in the case of  $\text{H}_2$  molecule.

In both cases, we will also discuss the level of entanglement between the two quantum subsystems, the electronic and nuclear components, providing additional insights into the nature of the proton transfer process.

### A. Test Systems

We chose the hydrogen molecule ( $\text{H}_2$ ) for testing the developed methodology, as the exact reference results are readily accessible and all possible types of interaction between particles such as electron-electron, proton-proton, and electron-proton are present. The NEO orbitals and corresponding integrals were prepared with the NEOHF method. For ease of calculation, the rather small split-valence double- $\zeta$  Gaussian basis set in 6-31 contraction scheme (6-31G) [73] basis set was used for the electronic orbitals and the nuclear orbitals were constructed using the smallest basis set available in GAMESS-US [66], split-valence double- $\zeta$  nuclear basis set composed of 2 uncontracted Cartesian  $S$  functions (DZSNB) [9]. For the showcase in Section IV B the electronic orbitals were constructed in single- $\zeta$  (minimal) basis set contracted from 6 Gaussian primitives (STO-6G). The basis set functions for electrons and nuclei

were centered at the positions corresponding to the experimental ground state structure [74] with an inter-nuclear distance equal to 0.7414 Å. We must stress that in general one must use the floating orbital approach [75–77], where the centers of the basis set functions are optimized to best fit the final wave function according to the variational principle. However, as it entails a more elaborate implementation we prefer to postpone this step and perform all tests with fixed orbital centers, similar to the studies performed in Refs. [78–81]. Note that our  $H_2$  Hamiltonian, similar to the work in Ref. [82], contains contributions from global translational and rotational motion. As these contributions increase the total energy they preferably must be eliminated [79, 83, 84]. We emphasize that our aim is not in delivering ultimate accuracy results but rather to establish the resource-efficient methodology for the quantum treatment of the electron-nuclear problem on near-term quantum computers. Based on the NEOHF orbitals the reference total energy has been evaluated with NEOFCI [9] method, see Table II. The same structure was used for the electronic Hartree–Fock (HF) calculation with a 6-31G basis set giving 4 orbitals for electrons. Consequently, these orbitals were used in Full Configuration Interaction (FCI) calculation for obtaining the reference energy. The reference energies for electronic and NEO cases are presented in Tables I and II, respectively.

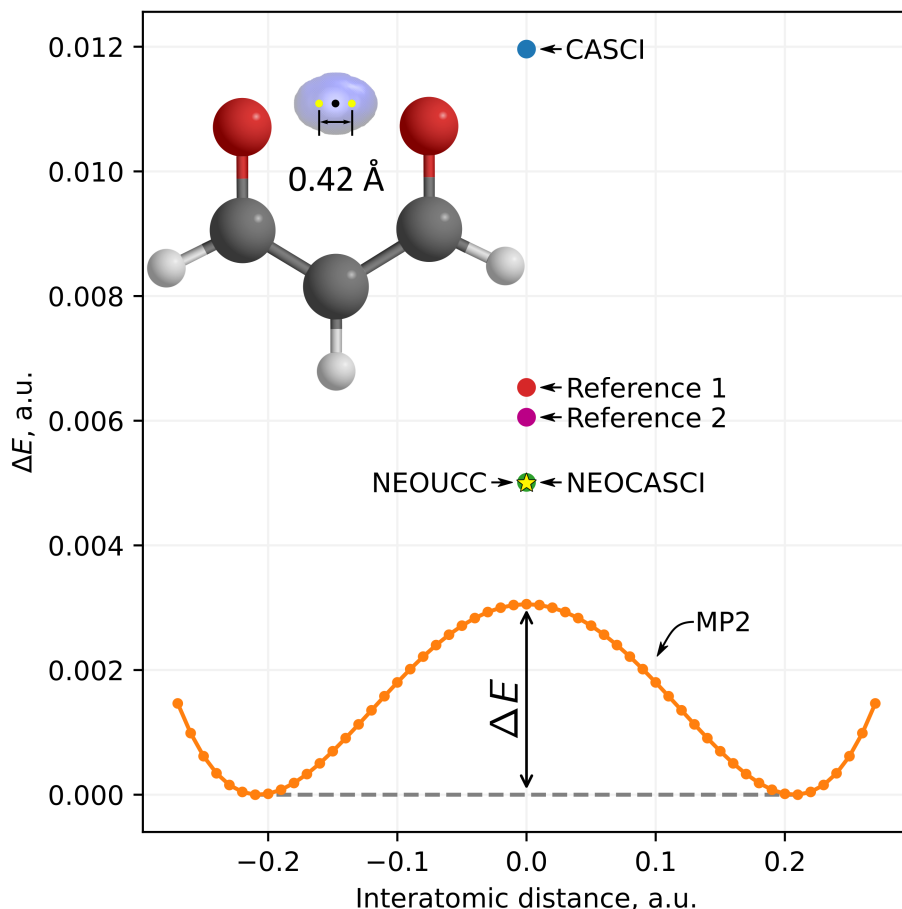


Figure 3: Potential energy surface for the proton translocation process in malonaldehyde. The curve in orange corresponds to a MP2 calculation, in which the tunneling proton (as all other atoms) is described as a classical point charge; it is given mainly as a guidance to the eyes. The path is simulated keeping all other atoms (but the moving proton) fixed in their original position. The structure of the malonaldehyde together with the first protonic NEOHF orbital (isosurface value  $10^{-4}$ ) are given in the upper inset. The distance between the equilibrium positions is found to be 0.42 Å. Both NEOCASCI (classical algorithm, green dot) and NEOUCC (quantum algorithm, yellow star) methods incorporate quantum proton effects and provide reasonable tunneling barrier values, while the classical description of the proton with CASCI (blue dot) leads to a considerable overestimation of the barrier. The values for “Reference 1” (red dot) and “Reference 2” (purple dot) are taken from Ref. [85] and Ref. [86] respectively.

For the second test system, we chose malonaldehyde. This molecule is an extensively studied benchmark system for quantum effects involving intramolecular hydrogen bonds. The key structural feature is the hydrogen bond O–H–O

for which there are two possible asymmetric configurations. This leads to a double-well potential with the states connected by proton tunneling. The experimental ground state structure [87] has  $C_s$  point group symmetry and the proton transfer occurs at a symmetric transition state structure in  $C_{2v}$  symmetry [9, 88]. To get a reasonable system for the description of the tunneling phenomena we first optimized the malonaldehyde structure using the second-order Møller–Plesset (MP2) method [89] in  $C_{2v}$  using the 6-31G basis set. The optimized structure corresponds to the transition state (TS) structure [9, 88]. After fixing all the coordinates but one, the search for minima was performed in  $C_s$  symmetry. This revealed two possible equilibrium locations for the proton separated from each other by 0.42 Å as well as the location of the barrier’s maximum. In Figure 3 one can see the equilibrium positions marked with yellow dots symmetrically located with respect to the position of the barrier maximum marked with a black dot. These coordinates were used as the centers for the nuclear basis functions for three different NEOHF calculations with DZSNB and 6-31G basis sets for nuclei and electrons respectively. Two NEOHF calculations were performed in  $C_{2v}$  symmetry representing TS place of nuclear orbitals (i) at equilibrium positions and (ii) at equilibrium together with the barrier’s maximum positions. The former will be referred to as “2-center  $C_{2v}$ ” and has 4 nuclear orbitals, while the latter, “3-center  $C_{2v}$ ”, has 6 nuclear orbitals.

The third NEOHF calculation represents the ground state, “1-center  $C_s$ ”, places nuclear orbitals at one of the equilibrium locations and has only 2 nuclear orbitals. In all cases, only one proton was treated quantum mechanically, while all other nuclei were taken as classical point charges. We also kept the same number of electronic orbitals resulting from the tunneling proton, placing them on all three centers (ghost atoms feature) for achieving an equal description of the electronic wave function in case of “1-center  $C_s$ ” and “3-center  $C_{2v}$ ” setups. Due to the presence of the classical nuclei, the NEO Hamiltonian does not contain the global rotational and translational degrees of freedom [90]. Based on the three sets of NEOHF orbitals (“1-center  $C_s$ ”, “2-center  $C_{2v}$ ”, “3-center  $C_{2v}$ ”) we have performed NEOCASI calculations in order to obtain the corresponding reference energies, see Table VII. To keep the electronic active space compact the 17 low-lying core orbitals for electrons were considered fully occupied and only 4 orbitals hosting 4 electrons were considered active in all calculations. For the nuclear active space, we used all 2 orbitals, 4 orbitals, and 6 orbitals for “1-center  $C_s$ ”, “2-center  $C_{2v}$ ”, and “3-center  $C_{2v}$ ” setups respectively. The reference results for NEOCASI are presented in Table VII while the electronic and nuclear NEOHF orbitals used in the active space for the NEOCASI calculation on “3-center  $C_{2v}$ ” setting are presented in Figure 4.

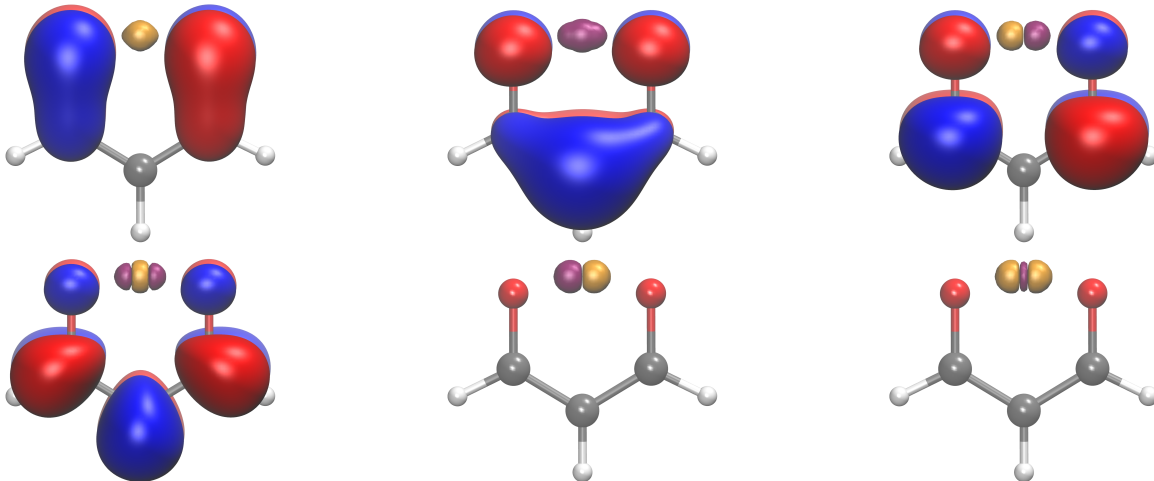


Figure 4: Electronic (red/blue) and nuclear (purple/orange) orbitals (isosurface value is 0.05) included in the active space of NEOCASI calculation for malonaldehyde in the “3-center  $C_{2v}$ ” setup. The orbitals have been prepared with a NEOHF calculation using a DZSNB and a 6-31G basis sets for the nuclei and the electrons, respectively.

## B. Initialization of the Electronic Parameters in NEO Ansatz

As discussed in Section II C, the choice of initial parameters in any VQE ansatz can have a significant influence on the convergence rate as well as the accuracy of a calculation. We show here that the optimized wave function of the electronic subsystem offers a good starting point to the NEO algorithm. As was already mentioned earlier the transfer of parameters between the electronic and NEO ansätze might need additional modifications if a point group symmetry is manifest. To this end, one needs to consider the different sign patterns occurring in the NEO and

electronic Hamiltonians after applying the  $\mathbb{Z}_2$ -symmetry reduction corresponding to a certain point group symmetry. We demonstrate this procedure on the example of the hydrogen molecule using NEOHF orbitals constructed with minimal size STO-6G and DZSNB basis sets for electrons and nuclei respectively as explained in Section IV A. Thus we keep the problem size small for illustration purposes and deal only with 4 orbitals for nuclei and 2 orbitals for electrons. This results in a NEO qubit Hamiltonian spanning 12 spin orbitals (8 nuclear spin orbitals and 4 electronic spin orbitals), while the electronic Hamiltonian spans just 4 spin orbitals. The  $\mathbb{Z}_2$ -symmetry arising from the  $D_{2h}$  point group symmetry of the electronic qubit Hamiltonian in parity mapping is given by the following operator

$$\mathbb{Z}_2^{\text{El.}} = IZIZ. \quad (38)$$

Applying tapering to the electronic Hamiltonian leads to a projection into the symmetry subspace corresponding to the HF state with  $\mathbb{Z}_2^{\text{El.}}$  eigenvalue equal to -1. Thus, after two-qubit reduction [72] and symmetry tapering the resulting electronic Hamiltonian will take the following form

$$\hat{H}_{\text{El.}} = -0.322833 \times I - 0.803007 \times Z - 0.180939 \times X. \quad (39)$$

For the NEO qubit Hamiltonian in parity encoding the corresponding  $\mathbb{Z}_2$ -symmetry is

$$\mathbb{Z}_2^{\text{NEO}} = IZZIZZZIZIZ. \quad (40)$$

However, in this case, the symmetry operator eigenvalue is +1. Thus the eigenvalue with a different sign will be incorporated into the Hamiltonian during the symmetry tapering. To reveal this effect, we further perform 4-qubit reduction according to Section III A and project the NEO Hamiltonian onto the electronic subspace. The corresponding projector,  $P_e$ , is similar to the one introduced in Section III B except that it additionally projects the NEO qubit Hamiltonian onto states where the nuclear alpha spin orbitals occupied according to the lowest NEOHF occupation. Thus the resulting NEO qubit Hamiltonian,

$$\hat{P}_e \hat{H}_{\text{NEO}} \hat{P}_e = -0.217313 \times I - 0.816590 \times Z + 0.181576 \times X, \quad (41)$$

is limited to the states where only the energetically lowest triplet NEOHF occupation for protons is allowed. One can clearly recognize in Eq. (41) that the off-diagonal term acquires a change of sign when compared to the electronic case, Eq. (39). This difference in the sign signature is also present for the parameters in the electronic and NEO ansätze. One way to solve this issue would be to perform a signature similarity transformation of the electronic Hamiltonian. For the specific case discussed here, this will correspond to

$$Z \hat{H}_{\text{El.}} Z = -0.322833 \times I - 0.803007 \times Z + 0.180939 \times X. \quad (42)$$

Since such a transformation is isospectral [91], one can use the transformed electronic Hamiltonian to find the parameters of the electronic ansatz, and then apply these parameters as an initial guess for the NEO ansatz. In this work, this “signature similarity transformation” is performed by comparing and fixing the signs of the Pauli words of the projected NEO Hamiltonian and of the electronic Hamiltonian according to the expressions in Eq. (39) and Eq. (41).

The similar weights (coefficients) obtained for the projected NEO and in the electronic Hamiltonians, Eq. (41) and Eq. (42), attests to the efficacy of the proposed parameter initialization methodology. However, before transferring electronic parameters to the NEO ansatz, it could be beneficial to additionally optimize them using the projected NEO Hamiltonian  $\hat{P}_e \hat{H}_{\text{NEO}} \hat{P}_e$  (Eq. (41)). More details will be given in Section IV C. In the following, we limit ourselves to the case of the initialization of the electronic parameters for the hardware-efficient ansatz for  $\text{H}_2$  in the minimal basis set. After performing symmetry tapering, 4-qubit reduction, and restricting to nuclear triplet states according to Sections III A and III B, one finally obtains a 4-qubit NEO Hamiltonian (See Appendix D, Eq. (D1)). The first qubit (of the 4-qubit register) corresponds to the electronic state, while the other 3 qubits describe the nuclear state (see Figure 5). One can initialize electronic parameters simply by transferring the wave function of the electronic subsystem into the NEO ansatz, as shown in Figure 5. All nuclear parameters must then be initialized to zero except for the second  $R_y$  gate on qubit  $q_1$ . In this specific case, it is set to  $\pi$  resulting in the lowest energy triplet nuclear occupation. This procedure, that we will denote “expanded”, can be easily generalized to larger system sizes. A second more economic variant only requires the additions of entangling gates between the electronic and the nuclear qubit subregisters, as shown in Figure 6. This variant, referred to as “stacked”, can be also generalized to larger systems and is advantageous in cases with weak entanglement between the protons. It is worth mentioning that for the electronic parameters (in blue color in Figure 6) to remain as close as possible to their initial values (*i.e.*, for avoiding the phase flip induced by the CZ gate) the number of entangling layers is required to be even.

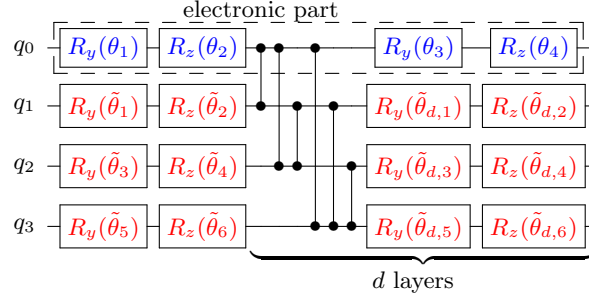


Figure 5: The “expanded” variant for the initialization of the electronic parameters in hardware-efficient ansatz. The circuit is designed for the case of 4-qubit NEO Hamiltonian, corresponding to  $H_2$  using minimal basis sets, STO-6G for electrons and DZSNB for nuclei. We use an “all-to-all” entangling scheme with CZ gates applied between all qubits. The electronic subsystem is delimited by a dashed box. Parameters in blue are initialized according to the results of the electronic subsystem optimization. All parameters in red:  $\tilde{\theta}_i$  ( $i = 1, 6$ ) and  $\tilde{\theta}_{d,i}$  ( $i = 1, 6$ ) are initialize to 0, with the exception of  $\tilde{\theta}_{d_{max},1}$ , which is set to  $\pi$  ( $d_{max}$  is the maximum number of repetitions). While for this specific case one entangling layer,  $d = 1$ , would be sufficient, for larger systems more layers will be required.

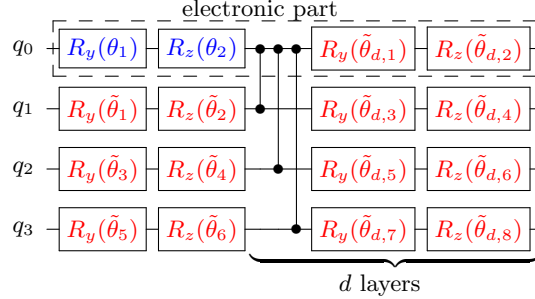


Figure 6: The “stacked” variant for the initialization of the electronic parameters in hardware-efficient ansatz. The circuit is designed for the case of 4-qubit NEO Hamiltonian, corresponding to  $H_2$  using minimal basis sets, STO-6G for electrons and DZSNB for nuclei. The electronic and nuclear parameters are shown in blue and red respectively. In this case, entangling CZ gates are only applied between electronic and nuclear subsystem qubits. The electronic subsystem is delimited by a dashed box. Parameters in blue are initialized according to the results of the electronic subsystem optimization. All parameters in red:  $\tilde{\theta}_i$  ( $i = 1, 6$ ) and  $\tilde{\theta}_{d,i}$  ( $i = 1, 8$ ) are initialized to 0, with the exception of  $\tilde{\theta}_1$ , which is set to  $\pi$ . Note that the number of layers,  $d$ , should be even in order for the electronic parameters to remain as close as possible to their initial values (*i.e.*, for avoiding the phase flip induced by the CZ gates).

### C. $H_2$ calculations

Initially, we have performed VQE optimization of the electronic UCCSD ansatz for the ground state of the  $H_2$  molecule employing an electronic Hamiltonian with classical nuclei,  $\hat{H}_{EL}$ . The final energy agrees well with the reference value obtained from FCI calculations, see Table I. To verify the validity of the electronic UCCSD parameters for the NEOUCCSD ansatz we employ the projected NEO Hamiltonian,  $P_e \hat{H}_{NEO} P_e$ , in a manner similar to Eq. (41) in Section IV B. After projection and tapering, the 5-qubit NEO Hamiltonian considers only states where the nuclear part corresponds to the lowest energy triplet nuclear NEOHF occupation and has the same size as the electronic qubit Hamiltonian. The corresponding ground state energy of 1.065040 Hartree has been calculated by exact diagonalization of  $P_e \hat{H}_{NEO} P_e$ . Initializing the electronic parameters in NEOUCCS<sup>(1,0)</sup>D<sup>(2,0)</sup> (see notation in Section II B) to the values from electronic UCCSD ansatz, we have evaluated the corresponding expectation value,  $\langle P_e \hat{H}_{NEO} P_e \rangle$ . One can see from Table I that the resulting expectation value approximates the ground state reference energy for  $P_e \hat{H}_{NEO} P_e$  within an error of less than  $10^{-4}$  Hartree. By letting the electronic parameters further relax in optimization employing the NEOUCCS<sup>(1,0)</sup>D<sup>(2,0)</sup> ansatz and  $P_e \hat{H}_{NEO} P_e$  one removes this error, recovering the exact reference energy, see Table I. Having resolved the reduced problem based on  $P_e \hat{H}_{NEO} P_e$  Hamiltonian we proceed to the full 8-qubit NEO

Table I:  $\text{H}_2$  ground state energies calculated with quantum computing ansätze (UCCSD and NEOUCCS<sup>(1,0)</sup>D<sup>(2,0)</sup>) and classical algorithms (FCI and “exact diagonalization”). Two Hamiltonians are used: the electronic Hamiltonian ( $\hat{H}_{\text{El.}}$ ) and the projected NEO Hamiltonian ( $P_e \hat{H}_{\text{NEO}} P_e$ ). The UCCSD electronic parameters reproducing the FCI wave function provide a good initial guess for NEOUCCS<sup>(1,0)</sup>D<sup>(2,0)</sup> ansatz (applied on  $P_e \hat{H}_{\text{NEO}} P_e$ ) with an error of  $8.35 \times 10^{-5}$  Ha. Further optimization of parameters (“relaxed”) recovers the ground state energy of the  $P_e \hat{H}_{\text{NEO}} P_e$  (“exact diagonalization”).

Hamiltonian		Method	Parameters	Energy/Ha
$\hat{H}_{\text{El.}}$		FCI		-1.151683
		UCCSD	electronic	-1.151683
$P_e \hat{H}_{\text{NEO}} P_e$		exact diagonalization		-1.065040
		NEOUCCS <sup>(1,0)</sup> D <sup>(2,0)</sup>	electronic	-1.064956
			relaxed	-1.065040

Hamiltonian. After symmetry tapering, 4-qubit reduction, and projection to the nuclear triplet state according to Sections III B and III A, the electronic state is spanned by 5 qubits, and 3 qubits are used for the nuclear state. The results for the VQE energy optimizations employing various types of NEOUCC parameterizations with advanced and ordinary parameter initialization are presented in Table II. For the advanced initialization procedure, we employ relaxed electronic parameters obtained with NEOUCCS<sup>(1,0)</sup>D<sup>(2,0)</sup> and  $P_e \hat{H}_{\text{NEO}} P_e$  as discussed above. All variants of the NEOUCC parameterization in Table II contain double and single excitations for nuclei and electrons, which will be indicated as

$$\text{SD} \equiv \text{S}^{(1,0)} \text{S}^{(0,1)} \text{D}^{(0,2)} \text{D}^{(1,1)} \text{D}^{(2,0)}. \quad (43)$$

If mixed electronic-nuclear double excitations are added then the resulting NEOUCCDD<sup>(1,1)</sup> ansatz deliver the results with an error below  $10^{-4}$  Hartree. The addition of the mixed triple,  $\text{T}^{(1,2)}$ , excitations in the NEOUCCSDD<sup>(1,1)</sup>T<sup>(1,2)</sup> ansatz does not decrease the error further. If instead, one adds the mixed triple excitation with double electronic excitation,  $\text{T}^{(2,1)}$ , the error decreases below  $5 \times 10^{-6}$  Hartree. Including both variants of mixed triple excitation brings the error below  $10^{-6}$  Hartree. It is clear that the  $\text{D}^{(1,1)}$  and the  $\text{T}^{(2,1)}$  operators are the primary contributors to the lowering of the energy, while the  $\text{T}^{(1,2)}$  operator has minimal effect. The difference in final NEOUCC energy

Table II: Ground state energies for the  $\text{H}_2$  NEO Hamiltonian obtained with different variants of the NEOUCC quantum computing ansatz and the COBYLA optimizer. In general, a good agreement with NEOF CI is reached for all variants, however, one should emphasize the importance of the  $\text{T}^{(2,1)}$  excitations in delivering excellent agreement with the reference. The calculations employ both “ordinary” and “advanced” initialization procedures, as described in Sec. IV B. Although the “advanced” initialization scheme improves slightly the accuracy, we expect more significant improvements in the case of a larger number of parameters.

		Method	Energy/Ha	iterations
Order		Initialization		
NEOUCC	SD	advanced	-1.066039	856
		ordinary	-1.066039	1341
	SDT <sup>(1,2)</sup>	advanced	-1.066039	1093
		ordinary	-1.066039	1674
	SDT <sup>(2,1)</sup>	advanced	-1.066120	1377
		ordinary	-1.066121	2179
	SDT	advanced	-1.066121	1074
		ordinary	-1.066120	3945
NEOF CI			-1.066121	

between optimizations with advanced initialization (set to relaxed electronic parameters) and ordinary initialization

(set to the NEOHF state) fall close to the convergence tolerance,  $\epsilon \leq 10^{-6}$  Hartree. For NEOUCC ansätze the advanced initialization scheme improves accuracy for the cases with a large number of variational parameters such as NEOUCCSDT. However, the main benefit lies in a faster convergence rate, in certain cases reaching a 4-fold speedup, see Table II. Additional analysis for convergence of NEOUCC ansatz using different initialization schemes can be found in Appendix B.

Table III presents the assessment for the contribution of each type of excitation operator to the correlation energy in NEO wave function. The correlation energy within the chosen basis set amounts to 0.024634 Hartree. If one uses double and single excitation operators for the protons only then energy can not decrease lower than NEOHF. Adding the single and double operators, NEOUCCSD, for electrons brings the energy nearly to the same value as for the case when only electronic operators are included, see Table III. This can be attributed to the low correlation between protons. However, the mixed electron-nuclear operators make a substantial contribution to the correlation energy. Specifically, addition of mixed double excitation,  $D^{(1,1)}$ , brings error below  $10^{-4}$  Hartree. If one also includes mixed triple operators,  $T^{(2,1)}$ , the error falls further below  $5 \times 10^{-6}$  Hartree. The ultimate accuracy of  $5 \times 10^{-7}$  Hartree is reached if all excitation operators up to triple-order are included.

Table III: The ground state energies for the  $H_2$  NEO Hamiltonian obtained with different variants of NEOUCC quantum computing ansatz and classical computational methods (NEOHF and NEOF CI). Increasing the excitation order in the NEOUCC ansatz lowers the error in the calculation. The mixed  $D^{(1,1)}$  nuclear-electron operators have a larger contribution to the correlation than T operators, while the mixed triple operators with higher electronic excitation order,  $T^{(2,1)}$ , play a more important role than  $T^{(1,2)}$ . The significance of pure nuclear operators is minimal.

	Method	Energy/Ha	Error/Ha
	NEOF CI	-1.066121	
	NEOHF	-1.041487	0.024634
NEOUCC	$S^{(0,1)}D^{(0,2)}$	-1.041487	0.024634
	$S^{(1,0)}D^{(2,0)}$	-1.065040	0.001082
	$S^{(1,0)}D^{(2,0)}D^{(1,1)}$	-1.066037	0.000084
	$S^{(1,0)}D^{(2,0)}T^{(2,1)}$	-1.065063	0.001059
	$S^{(1,0)}D^{(2,0)}D^{(1,1)}T^{(2,1)}$	-1.066117	0.000004
	$SD^{(2,0)}D^{(0,2)}$	-1.065049	0.001073
	$SDT^{(2,1)}$	-1.066121	0.000001
	SDT	-1.066121	0.000001

We supplement our study of the correlation nature in the  $H_2$  molecule with the measure of entanglement entropy. Specifically, we evaluate the entanglement between electronic and nuclear subsystems, according to Section II D. We find that the entanglement for the  $H_2$  molecule at equilibrium based on the NEOF CI wave function amounts to 0.0069. The same value can be accurately reproduced with the NEOUCC ansatz (see Table IV) when quadruple excitation operators are included. To monitor the change in entanglement upon dissociation, we also evaluated NEOF CI entropies for distances of 1.9582 Å and 3.1751 Å. Note that these quantities correspond to the separation between the centers hosting the nuclear and electronic orbitals and are taken as an approximated measure of the inter-atomic distance. Table IV shows how the entanglement between electron and proton subsystems (according to NEOF CI) strengthens to 0.0103 during the “bond extension” and then slightly declines to 0.0097 after “dissociation”. The corresponding NEOUCC results are in good agreement with the reference calculations, demonstrating the reliability of the NEOUCC approach.

Although a UCC type ansatz can be very accurate, in general, they cannot yet be efficiently utilized on current quantum hardware. Thus we present an optimal strategy for the application of the TwoLocal ansatz with NEO Hamiltonian employing parameter initialization procedures discussed in Section IV B. Similar to the NEOUCC case we first optimized the TwoLocal ansatz for the electronic Hamiltonian and relaxed electronic parameters further, employing the  $P_e \hat{H}_{\text{NEO}} P_e$  Hamiltonian. For both Hamiltonians we used TwoLocal ansatz with 8 entangling layers, see Figure 2 and Figure 5. As can be seen from Table V the TwoLocal ansatz performs similarly to the NEOUCC ansatz both in terms of accuracy and the validity of the advanced parameter initialization. However, the 8-qubit NEO Hamiltonian represents a difficult optimization case for the TwoLocal ansatz with 8 entangling layers if ordinary parameter initialization is used. Initial guess parameters are usually set randomly which often can not even deliver optimized energy below the NEOHF energy. One can see from Table VI that for the best optimization case, the error is still larger than for 5-qubit TwoLocal ansatz applied on  $P_e \hat{H}_{\text{NEO}} P_e$ .

Table IV: Von Neumann entropy between the electronic and nuclear subspaces (Sec. IID) at three points along the  $H_2$  dissociation curve. The entropy increases with the extension of the bond length and then slightly declines upon dissociation. Increasing the order of excitations in the quantum computing NEOUCC ansatz, one can accurately reproduce the reference value obtained with the classical approach, NEOFCI.

		Separation		
Method		0.7414 Å	1.9582 Å	3.1751 Å
NEOFCI		0.0069	0.0103	0.0097
NEOUCC	SD	0.0062	0.0050	0.0037
	SDT	0.0068	0.0104	0.0098
	SDTQ	0.0068	0.0104	0.0098

If one sets the initial guess to the relaxed electronic parameters in TwoLocal ansatz according to the “expanded” variant with 8 entangling layers, see Figures 2 and 5, the energy decreases slightly below the ground state energy for the  $P_e \hat{H}_{\text{NEO}} P_e$  Hamiltonian. Although the “expanded” variant of the electronic parameter initialization delivers lower energy than ordinary optimization the error amounts to  $10^{-3}$  Hartree. Expanding the relaxed electronic 5-qubit TwoLocal ansatz with 3 nuclear qubits we continue stacking entangling layers between electronic and nuclear qubits only according to Section IV B. This “stacked” variant of electronic parameter initialization, Figure 6, performs better, see Table VI, giving an error of about  $2 \times 10^{-4}$  Hartree when 14 stacked layers are used. Although the proper parameter initialization requires an even number of stacked electronic-nuclear entangling layers the cases with an odd number perform equally well. Initial energy in VQE optimization is above NEOHF energy if an odd number of entangling layers is used whereas, for an even number, it is exactly the ground state energy for  $P_e \hat{H}_{\text{NEO}} P_e$ . Obviously, it did not affect the VQE optimization using the CG and SLSQP. It should be also noted that CG optimizer performed best in the case of TwoLocal ansatz, while SLSQP and COBYLA deliver similar results.

Table V:  $H_2$  ground state energies calculated with the TwoLocal and two classical approaches: FCI and “exact diagonalization”. Two Hamiltonians are used: the electronic Hamiltonian ( $\hat{H}_{\text{El.}}$ ) and the projected NEO Hamiltonian ( $P_e \hat{H}_{\text{NEO}} P_e$ ). The TwoLocal electronic parameters reproducing the FCI wave function provide a good initial guess for the NEO calculation with the Hamiltonian  $P_e \hat{H}_{\text{NEO}} P_e$ , leading to an error of  $8.35 \times 10^{-5}$  Ha. Further optimization of parameters (“relaxed”) reduces the error to  $3.83 \times 10^{-7}$  Ha compared to the ground state energy of the  $P_e \hat{H}_{\text{NEO}} P_e$  (“exact diagonalization”).

Hamiltonian	Method	Parameters	Energy/Ha
$\hat{H}_{\text{El.}}$	FCI		-1.151683
	TwoLocal	electronic	-1.151683
$P_e \hat{H}_{\text{NEO}} P_e$	exact diagonalization		-1.065040
	TwoLocal	electronic	-1.064956
	TwoLocal	relaxed	-1.065039

#### D. Malonaldehyde

We start our malonaldehyde investigation with the “2-center  $C_{2v}$ ” setup, which corresponds to the situation in which the proton is equally shared between the two oxygen atoms (see Figure 3). A similar setup was already proposed in Ref. [9] for the evaluation of double well splitting. However, our aim is different and consists mainly in providing benchmark results (more specifically, ground state energies) for the validation of the quantum NEO algorithm. Using the same transformations as in Section IV C, we converted the second quantized Hamiltonian based on 16 spin orbitals to an 8-qubit Hamiltonian, 5 qubits spanning the electronic subspace, and 3 qubits spanning the nuclear one. Increasing excitation order from double to quadruple in the NEOUCC ansatz, we could recover the NEOCASCI reference results and reach  $10^{-6}$  Hartree accuracy, as shown in Table VII. The results for the entanglement entropy are presented in Table VII and are also in very good agreement with the reference values.

Table VI: Ground state energies for the  $H_2$  NEO Hamiltonian obtained with various implementations of the TwoLocal quantum ansatz and with the classical NEOF CI approach. The “advanced” initialization scheme for electronic parameters performs significantly better than the “ordinary” one for both CG and SLSQP optimizers. The “stacked” initialization with 14 entangling layers delivers the most accurate result with an error of  $2 \times 10^{-4}$  Ha using the CG optimizer.

Method		Layers	Energy/Ha	
			SLSQP	CG
Ordinary			-1.013923	-1.014310
Expanded			-1.065054	-1.065172
TwoLocal	Stacked	$d = 3$	-1.065175	-1.065633
		$d = 4$	-1.065056	-1.065381
		$d = 10$	-1.065055	-1.065663
		$d = 11$	-1.064975	-1.065814
		$d = 12$	-1.065055	-1.065720
		$d = 13$	-1.064939	-1.065691
		$d = 14$	-1.065054	-1.065889
		$d = 20$	-1.065056	-1.065666
NEOF CI			-1.066121	

For evaluation of the tunneling barrier, we used the “3-center  $C_{2v}$ ” (top of the barrier) and “1-center  $C_s$ ” (bottom of the potential, see Figure 3) setups as described in Section IV A. Based on the NEOCASCI calculations at these two setups, the barrier is estimated to be 0.005011 Hartree. This is rather close to the values obtained in Ref. [85] (full dimensional calculations with near basis-set-limit frozen-core CCSD(T)) and Ref. [86] (*in silico* transient X-ray absorption spectroscopy) of 0.0065 Hartree and 0.0061 Hartree, respectively. On the other hand, using a fully classical approach such as Complete Active Space Configuration Interaction (CASCI) for the evaluation of the barrier, we observed a severe overestimation of the barrier, which reaches a value of 0.01196 Hartree (see Figure 3 and table VII). Note that in Figure 3 we also report the full potential energy surface computed with MP2 and a classical proton. However, at this small basis set size for the expansion of the electronic wave function, we can only expect a qualitative description of the process, which we only report as guidance for the reader’s eyes. To account for nuclear quantum effects, we repeat the same calculation using our proposed NEOUCC algorithm. In this setup, the qubit Hamiltonian for the “3-center  $C_{2v}$ ” setup is spanned by 10 qubits, 5 qubits for electronic subspace and 5 qubits for nuclear subspace. The “1-center  $C_s$ ” qubit Hamiltonian is instead spanned by 7 qubits, 6 qubits for electronic subspace and 1 qubit for nuclear subspace. The energies for both systems estimated with various NEOUCC schemes are presented in Table VII. Already with a rather modest NEOUCCSD ansatz, we observe very good agreement with the NEOCASCI reference, with a deviation smaller than  $10^{-4}$  Hartree. The error decreases upon inclusion of higher order excitation operators in NEOUCC and gets below  $2 \times 10^{-6}$  Hartree for NEOUCCSDTQ. These calculations confirm the quality and the potential of the NEOUCC ansatz for the calculation of quantum nuclei effects and prove its fast convergence towards the exact solution.

In Table VII we summarize the values for the barrier energies together with the ones for the von Neumann entropy,  $s_n$  (Eq. (30)), associated with the entanglement between the nuclear and electronic subsystems. Also in this case the NEOUCC results are in very good agreement with the NEOCASCI references for all settings: “1-center  $C_s$ ”, “2-center  $C_{2v}$ ”, and “3-center  $C_{2v}$ ”. Assuming that the estimate for the  $C_s$  system is not very sensitive to the basis set size, our calculations support the picture in which the level of electron-nuclear entanglement increases as the proton is transferred to the top of the barrier (however, this observation can not be conclusive in view of the small basis set used for the electronic and nuclear problem, as well as of the rigidity imposed to the molecular scaffold). Further investigations are needed to shed light on the convergence of the entanglement entropy between electronic and nuclear subsystems as a function of the nuclear basis set size.

## V. DISCUSSION AND CONCLUSIONS

In this work, we developed and demonstrated a quantum algorithm for the treatment of quantum nuclear degrees of freedom on near-term quantum computers, based on the NEO approach [9]. This approach allows the description

Table VII: Energies and von Neumann entropies,  $s_n$  (Eq. (30)), of malonaldehyde obtained with different NEOUCC parameterizations and NEO Hamiltonians based on “3-center  $C_{2v}$ ”, “2-center  $C_{2v}$ ”, and “1-center  $C_s$ ” setups. The barrier height,  $\Delta E$ , is evaluated based on the difference between energies corresponding to “3-center  $C_{2v}$ ” and “1-center  $C_s$ ” setups. We observe good agreement with barrier height obtained in Ref. [85] and Ref. [86] for all variants of NEOUCC, while the electronic CASCI method severely overestimates it.

	“1-center $C_s$ ”		“2-center $C_{2v}$ ”		“3-center $C_{2v}$ ”			
Method	Energy/Ha	Entropy	Energy/Ha	Entropy	Energy/Ha	Entropy	$\Delta E$ /Ha	
Ref. [85]							0.006534	
Ref. [86]							0.006056	
CASCI	-265.528820				-265.516859		0.011962	
NEOCASCI	-265.490948	0.0000	-265.452062	0.0866	-265.485937	0.0044	0.005011	
NEOUCC	SD	-265.490685	0.0000	-265.451123	0.0616	-265.485761	0.0031	0.004924
	SDT	-265.490943	0.0000	-265.452051	0.0862	-265.485936	0.0044	0.005007
	SDTQ	-265.490947	0.0000	-265.452062	0.0866	-265.485939	0.0045	0.005009

of both components of molecular systems, *i.e.*, electrons and nuclei, at the same footing, namely at a quantum level, enabling the correct description of important nuclear quantum effects such as proton tunneling and non-adiabatic effects. From the quantum computing perspective, a quantum treatment of the full molecular wave function gives us the opportunity to extend the potential exponential quantum advantage already investigated for the electronic subsystem to the multi-component electron-nuclear wave function. In addition, this method will enable a rigorous estimation of the level of entanglement between the electronic and nuclear subsystems, providing a new and interesting tool for the understanding of post-BO effects. In order to make our approach more suited to near-term quantum computing, we implemented an embedding scheme, which allows the restriction of the nuclear quantum wave function to a selected number of atoms, while keeping the rest of the nuclei described at a classical level (*i.e.*, as point charges).

The ability of NEOUCC ansätze to deliver the ground state energy in noiseless VQE calculation was proven in two main applications: the hydrogen molecule, and malonaldehyde. In the latter case, only the shared proton between the two carbonyl groups was “quantized” while all other nuclei in the molecules were treated classically. Our results agree with conventional NEOF CI and NEOCASCI calculations to within an error of about  $10^{-6}$  Hartree.

Our NEOUCC calculations revealed that apart from the high contribution to the correlation energy from interactions between electrons, a substantial part of correlation energy is attributed to electron-nuclear interaction. Specifically, double electron-nuclear excitations are required for reducing the error below  $10^{-4}$  Hartree, and only after the addition of triplet  $T^{(2,1)}$  excitations, one can reach an accuracy of about  $10^{-6}$  Hartree. The importance of nuclear-electron quantum correlations is also demonstrated by the significant amount of nuclear-electron von Neumann entropy, which increases at bond breaking.

Moreover, we investigated the possibility of utilizing hardware-efficient ansätze as more compact representations of the NEO wave functions. We showed that the parameter initialization scheme plays an important role in the optimization process. Namely, to reach an accuracy below  $5 \times 10^{-4}$  Hartree, we introduced several ways of initialization of the NEO electronic wave function parameters from the converged electronic calculation. Such an efficient initialization procedure is not restricted to the use of hardware-efficient ansätze, and can also significantly increase convergence in the case of NEOUCC wave functions. In addition, the same scheme can also be employed beyond the typical cases for which the BO separation is employed, for instance in the case of weakly interacting molecular fragments.

Furthermore, we introduced a scheme for reducing the dimensionality of the effective Hamiltonian through the exploitation of those symmetries inherent in the NEO approach. Specifically, we have generalized the two-qubit reduction, already employed for the electronic wave function, extending it to the nuclear subsystem. The dimensionality of the nuclear Hilbert space is further reduced by leveraging the point group symmetry inherent in the molecular system. As this last step might have undesired consequences on the initialization of the electronic parameter, we have introduced and discussed a procedure for resolving the issue. In the last step, when dealing with nuclei of the same spin polarization we can additionally project out unpopulated spin orbitals from the Hamiltonian and remove corresponding qubits. This was demonstrated in this work for both orthohydrogen spin isomer and malonaldehyde with a single proton described as a quantum particle. Thus, for the qubit Hamiltonian in the case of orthohydrogen, we succeeded in reducing the number of qubits from 16 to 8. Similarly, for the malonaldehyde instead of using a 20-qubit Hamiltonian, we demonstrated the possibility to safely reduce the system to an effective 10-qubit Hamiltonian.

Reduction in the number of qubits leads to a significant decrease in the number of two-qubit entangling gates in the ansatz as well as the total number of terms in Hamiltonian required for measurement in VQE, making the entire algorithm more suited for near-term hardware calculations.

In conclusion, we have proposed and implemented a resource-efficient quantum algorithm for the simulation of molecular systems, where both electrons and nuclei are treated quantum mechanically within the NEO approach. Although the execution of the proposed NEO/VQE algorithm on state-of-the-art quantum hardware for systems of the size of malonaldehyde (with one quantum hydrogen atom) and orthohydrogen (with two quantum hydrogen atoms) is still premature, the developed machinery allowed us to benchmark our approach using VQE state vector simulations. By means of our applications, we could show the reliability and versatility of the NEOUCC ansatz, which is able of capturing nuclear-electron wave function energies and subsystem entropies with controlled accuracy. In particular, we demonstrated the possibility to evaluate the tunneling barrier for malonaldehyde with increasing accuracy by incorporating quantum nuclear effects into the calculation with the proposed NEOUCC algorithm. Building on these very promising initial results, we aim in the future to further generalize this framework by including sampling techniques and the possibility of investigating quantum electron-proton dynamics, opening up — thanks to the favorable scaling of the proposed quantum algorithm ( $\mathcal{O}(N_b^e + N_b^n)^4$ , where  $N_b^e$  and  $N_b^n$  are the numbers of basis set functions for electrons and nuclei respectively) — new avenues in the study of nuclear quantum effects in catalysis.

## VI. ACKNOWLEDGEMENTS

This work was supported by the Hartree National Centre for Digital Innovation, a collaboration between STFC and IBM. The authors thank Lars Tornberg for the helpful discussions. This research was supported by funding from Horizon 2020 via NEASQC project (grant number 951821), Wallenberg Center for Quantum Technology (WACQT), and from the NCCR MARVEL, a National Centre of Competence in Research, funded by the Swiss National Science Foundation (grant number 205602). IBM, the IBM logo, and ibm.com are trademarks of International Business Machines Corp., registered in many jurisdictions worldwide. Other product and service names might be trademarks of IBM or other companies. The current list of IBM trademarks is available at <https://www.ibm.com/legal/copytrade>.

### Appendix A: Single orbital entropy and quantum information

Single orbital entropies [92, 93] are calculated as

$$so_i = - \sum_{\alpha=1}^4 \omega_{i,\alpha} \ln(\omega_{i,\alpha}), \quad (\text{A1})$$

where  $\omega_{i,\alpha}$  are the eigenvalues of the one-orbital reduced density matrix [93, 94], the index  $i$  runs over molecular orbitals, and  $\alpha$  runs over the four possible occupations:  $--$ ,  $-\uparrow, \downarrow-$ ,  $\uparrow\downarrow$ . The sum over all single orbital entropies, the total quantum information [93], is given by

$$QI = \sum_i so_i. \quad (\text{A2})$$

The results for  $\text{H}_2$  (studied in Section IV C) and malonaldehyde in “2-center  $C_{2v}$ ” setting (studied in Section IV D) are shown in Tables VIII and IX.

### Appendix B: Parameter initialization and convergence

Figure 7 shows the different convergence profiles for the optimizations using “advanced” and “ordinary” initialization schemes with the NEOUCC ansätze and the COBYLA optimizer. As expected, we notice a faster convergence when the parameters precomputed for the electronic subsystem are transferred to the NEOUCC ansatz (Figure 7). Also, the initial energy values for the “advanced” initialization are lower than the ones using the “ordinary” initialization. In addition, our calculations show that as the complexity (and therefore the accuracy) of the ansatz increases, the effect of “advanced” initialization of the parameters becomes more important. Specifically, the convergence rate decreases upon the addition of triple excitations in going from NEOUCCSD, Figure 7a, to NEOUCCSDT<sup>(2,1)</sup> and NEOUCCSDT<sup>(1,2)</sup>, Figures 7c and 7b, respectively. Even though the number of electronic parameters is the same in both initialization procedures, the benefit of the ‘advanced’ procedure is indisputable, especially for the NEOUCCSDT ansatz where the convergence rate is increased more than threefold.

Table VIII: The single orbital entropies,  $so_i$ , and quantum information (total, electronic, and nuclear) for  $H_2$  (studied in Section IV C) evaluated with NEOUCCSDT.

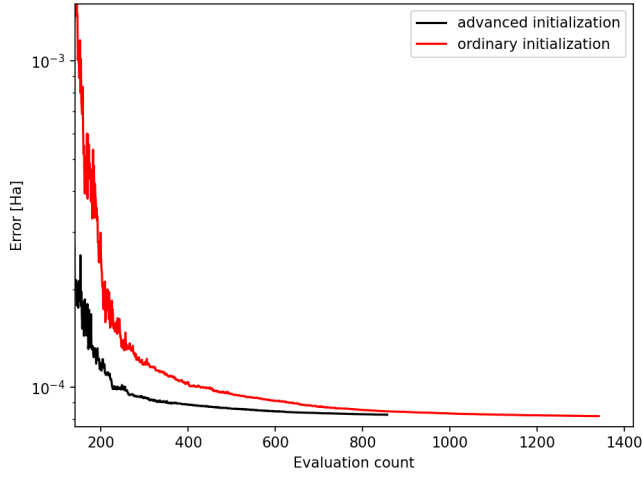
	orbital	$so_i$
electronic	1	0.0793
	2	0.0630
	3	0.0221
	4	0.0397
	$QI(\text{electronic})$	0.2041
nuclear	5	0.0035
	6	0.0035
	7	0.0035
	8	0.0035
	$QI(\text{nuclear})$ ( $\approx 6.4\%$ )	0.0139
	$QI(\text{total})$	0.2179

Table IX: The single orbital entropies,  $so_i$ , and quantum information (total, electronic, and nuclear) for malonaldehyde (“2-center  $C_{2v}$ ” setup) evaluated with NEOUCCSDTQ.

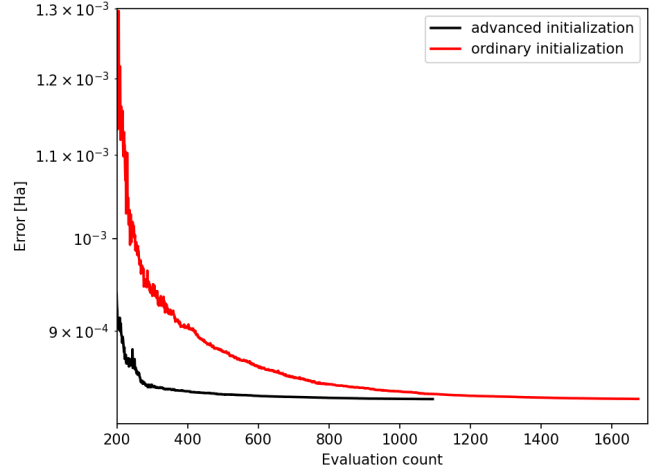
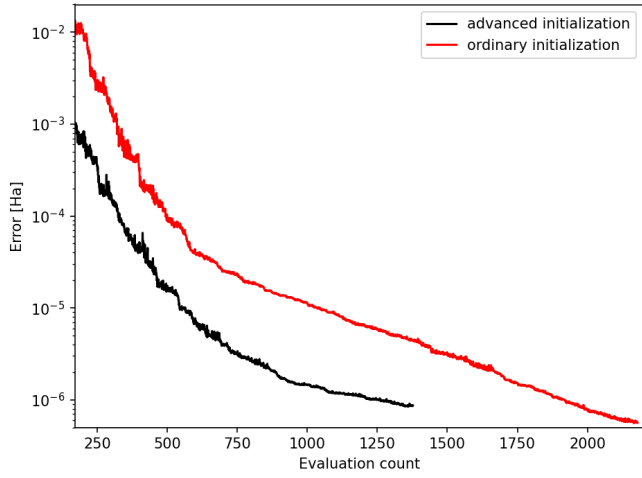
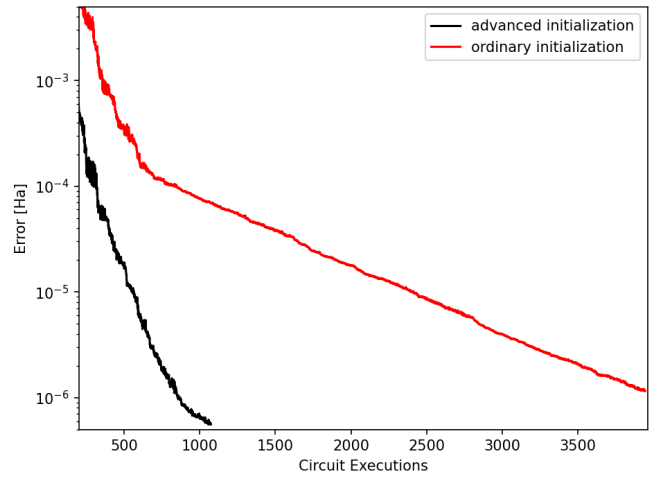
	orbital	$so_i$
electronic	1	0.0896
	2	0.1955
	3	0.2049
	4	0.0806
	$QI(\text{electronic})$	0.5705
nuclear	5	0.0867
	6	0.0866
	7	0.0000
	8	0.0001
	$QI(\text{nuclear})$ ( $\approx 23\%$ )	0.1734
	$QI(\text{total})$	0.7440

### Appendix C: Resource estimation

Both the number of qubits and the depth of the quantum circuit play a crucial role in determining the performance of quantum algorithms in near-term quantum computers. It is therefore important to analyze the hardware requirements needed to implement our quantum algorithm. As for the quantum gates, the number of entangling gates can strongly impact the circuit noise. In Table X we summarize the number of qubits, two-qubit entangling gates, and terms in the qubit Hamiltonian needed for the implementation of a VQE calculation for  $H_2$ , as reported in Section IV C. Specifically, these numbers refer to the final counts obtained after applying three different reduction schemes sequentially: (i) four-qubit tapering, (ii) point group (PG) symmetry, and (iii) projection onto a selected spin state. As wave function ansätze we employ TwoLocal (8 layers for the electronic part and 14 nuclear-electronic entangling layers) and NEOUCCSD, since they showed similar accuracy (see Section IV C). With the proposed schemes, we achieved a significant reduction — compared to the standard procedure — in the number of qubits and Hamiltonian terms, as well as in the number of entangling gates, for both ansätze.



(a) NEOUCCSD

(b) NEOUCCSDT<sup>(1,2)</sup>(c) NEOUCCSDT<sup>(2,1)</sup>

(d) NEOUCCSDT

Figure 7: Energy convergence plots for the  $H_2$  molecule with different NEOUCC ansätze and two initialization schemes. The classical optimization of the circuit parameters is done employing the COBYLA optimizer. The “advanced” initialization scheme introduced in Section II C (red lines) clearly outperforms the “ordinary” initialization procedure (black lines) for what concerns the speed of convergence, especially for large number of parameters (with SDT excitations).

Table X: Estimated resource requirements for the H<sub>2</sub> molecule (see Section IV C) using various reduction schemes. Shown are the number of qubits, two-qubit gates in TwoLocal as well as in NEOUCCSD ansätze, and the number of Pauli terms ( $|\{H\}|$ ) in the encoded Hamiltonian. All values are calculated using parity encoding. For the TwoLocal ansatz, 8 electron-to-electron entangling layers are applied to the electronic subsystem together with 14 electron-to-proton entangling layers.

Reduction	# Qubits	# Two-qubit Gates		$ \{H\} $
		TwoLocal	NEOUCCSD	
None	16	968	2546	861
+Four-qubit	12	558	2204	828
+PG symmetry	11	465	1472	825
+Spin projection	8	255	1202	428

#### Appendix D: NEO qubit Hamiltonian for H<sub>2</sub> in minimal basis set

$$\begin{aligned}
\hat{H}_{\text{NEO}} = & 1.697878 \times IIII - 0.373036 \times ZIII + 0.356877 \times IZII - 0.373036 \times ZZII - 0.337003 \times IIZI \\
& + 1.105641 \times ZIZI - 0.337002 \times IZZI + 1.094360 \times ZZZI - 0.416401 \times IIIZ + 0.004053 \times ZIIZ \\
& + 0.004053 \times ZZIZ - 0.004053 \times IIZZ - 0.004053 \times IZZZ + 0.416401 \times ZZZZ + 0.174434 \times XIII \\
& - 0.174434 \times XZII - 0.006416 \times IXII + 0.006416 \times ZXZI - 0.004740 \times YYII - 0.004740 \times XXZI \\
& + 0.004740 \times YYIZ + 0.004740 \times XXZZ - 0.186061 \times IIXI + 0.186061 \times IZZI - 0.748764 \times XIXI \\
& + 0.748764 \times XZXI + 0.004740 \times ZXXI + 0.004740 \times IYYI - 0.004740 \times ZXXZ - 0.004740 \times IYYZ \\
& - 0.006416 \times XXXI - 0.006416 \times YXYI + 0.181576 \times IIIX + 0.174434 \times XIIX - 0.174434 \times XZIX \\
& - 0.006416 \times IXIX + 0.006416 \times ZXZX - 0.186061 \times IIXX + 0.186061 \times IZXX - 0.006416 \times XXXX \\
& - 0.006416 \times YXYX
\end{aligned} \tag{D1}$$

- 
- [1] Thomas E Markland and Michele Ceriotti. Nuclear quantum effects enter the mainstream. *Nature Reviews Chemistry*, 2(3):1–14, 2018.
  - [2] Leonid Pereyaslavets, Igor Kurnikov, Ganesh Kamath, Oleg Butin, Alexey Illarionov, Igor Leontyev, Michael Olevanov, Michael Levitt, Roger D Kornberg, and Boris Fain. On the importance of accounting for nuclear quantum effects in ab initio calibrated force fields in biological simulations. *Proceedings of the National Academy of Sciences*, 115(36):8878–8882, 2018.
  - [3] Derren J Heyes, Michiyo Sakuma, Sam P de Visser, and Nigel S Scrutton. Nuclear quantum tunneling in the light-activated enzyme protochlorophyllide oxidoreductase. *Journal of Biological Chemistry*, 284(6):3762–3767, 2009.
  - [4] Mariana Rossi, Piero Gasparotto, and Michele Ceriotti. Anharmonic and quantum fluctuations in molecular crystals: A first-principles study of the stability of paracetamol. *Physical Review Letters*, 117(11):115702, 2016.
  - [5] Alexandra Vardi-Kilshstein, Neta Nitoker, and Dan Thomas Major. Nuclear quantum effects and kinetic isotope effects in enzyme reactions. *Archives of Biochemistry and Biophysics*, 582:18–27, 2015.
  - [6] Simone Raugé and Michael L Klein. Nuclear quantum effects and hydrogen bonding in liquids. *Journal of the American Chemical Society*, 125(30):8992–8993, 2003.
  - [7] Kyung Hwan Kim, Harshad Pathak, Alexander Späh, Fivos Perakis, Daniel Mariedahl, Jonas A Sellberg, Tetsuo Katayama, Yoshihisa Harada, Hirohito Ogasawara, Lars GM Pettersson, et al. Temperature-independent nuclear quantum effects on the structure of water. *Physical Review Letters*, 119(7):075502, 2017.
  - [8] Bet Pamuk, Jose M Soler, R Ramírez, CP Herrero, PW Stephens, PB Allen, and M-V Fernández-Serra. Anomalous nuclear quantum effects in ice. *Physical Review Letters*, 108(19):193003, 2012.
  - [9] Hammes-Schiffer S. Webb S. P., Iordanov T. Multiconfigurational nuclear-electronic orbital approach: Incorporation of nuclear quantum effects in electronic structure calculations. *J. Chem. Phys.*, 117:4106–4118, 2002.
  - [10] Benjamin Simmen, Edit Mátyus, and Markus Reiher. Elimination of the translational kinetic energy contamination in pre-Born–Oppenheimer calculations. *Molecular Physics*, 111(14-15):2086–2092, 2013.
  - [11] Hiromi Nakai. Simultaneous determination of nuclear and electronic wave functions without born–oppenheimer approximation: Ab initio no+mo/hf theory. *International Journal of Quantum Chemistry*, 86(6):511–517, 2002.
  - [12] Seunghoon Lee, Joonho Lee, Huanchen Zhai, Yu Tong, Alexander M. Dalzell, Ashutosh Kumar, Phillip Helms, Johnnie Gray, Zhi-Hao Cui, Wenyuan Liu, Michael Kastoryano, Ryan Babbush, John Preskill, David R. Reichman, Earl T.

- Campbell, Edward F. Valeev, Lin Lin, and Garnet Kin-Lic Chan. Is there evidence for exponential quantum advantage in quantum chemistry? *arXiv:2208.02199*, 2022.
- [13] Morten Kjaergaard, Mollie E Schwartz, Jochen Braumüller, Philip Krantz, Joel I-J Wang, Simon Gustavsson, and William D Oliver. Superconducting qubits: Current state of play. *Annual Review of Condensed Matter Physics*, 11:369–395, 2020.
- [14] He-Liang Huang, Dachao Wu, Daojin Fan, and Xiaobo Zhu. Superconducting quantum computing: a review. *Science China Information Sciences*, 63(8):1–32, 2020.
- [15] R. Somma, G. Ortiz, J. E. Gubernatis, E. Knill, and R. Laflamme. Simulating physical phenomena by quantum networks. *Phys. Rev. A*, 65:042323, Apr 2002.
- [16] Dave Wecker, Matthew B. Hastings, Nathan Wiebe, Bryan K. Clark, Chetan Nayak, and Matthias Troyer. Solving strongly correlated electron models on a quantum computer. *Phys. Rev. A*, 92:062318, Dec 2015.
- [17] Bela Bauer, Dave Wecker, Andrew J. Millis, Matthew B. Hastings, and Matthias Troyer. Hybrid quantum-classical approach to correlated materials. *Phys. Rev. X*, 6:031045, Sep 2016.
- [18] Adam Smith, M. S. Kim, Frank Pollmann, and Johannes Knolle. Simulating quantum many-body dynamics on a current digital quantum computer. *npj Quantum Information*, 5(1):106, November 2019.
- [19] Chris Cade, Lana Mineh, Ashley Montanaro, and Stasja Stanisic. Strategies for solving the fermi-hubbard model on near-term quantum computers. *Phys. Rev. B*, 102:235122, Dec 2020.
- [20] A. Chiesa, F. Tacchino, M. Grossi, P. Santini, I. Tavernelli, D. Gerace, and S. Carretta. Quantum hardware simulating four-dimensional inelastic neutron scattering. *Nature Physics*, 15(May 2019):455–459, March 2019.
- [21] F. Tacchino, A. Chiesa, S. Carretta, and D. Gerace. Quantum computers as universal quantum simulators: State-of-the-art and perspectives. *Advanced Quantum Technologies*, 3(3):1900052, 2020.
- [22] Philippe Suchsland, Panagiotis Kl. Barkoutsos, Ivano Tavernelli, Mark H. Fischer, and Titus Neupert. Simulating a ring-like hubbard system with a quantum computer. *arXiv:2104.06428*, 2021.
- [23] Alexander Miessen, Pauline J. Ollitrault, and Ivano Tavernelli. Quantum algorithms for quantum dynamics: A performance study on the spin-boson model. *Phys. Rev. Research*, 3:043212, Dec 2021.
- [24] Francesco Libbi, Jacopo Rizzo, Francesco Tacchino, Nicola Marzari, and Ivano Tavernelli. Effective calculation of the green’s function in the time domain on near-term quantum processors. *Phys. Rev. Res.*, 4:043038, Oct 2022.
- [25] Jacopo Rizzo, Francesco Libbi, Francesco Tacchino, Pauline J. Ollitrault, Nicola Marzari, and Ivano Tavernelli. One-particle green’s functions from the quantum equation of motion algorithm. *Phys. Rev. Res.*, 4:043011, Oct 2022.
- [26] E. A. Martinez, C. A. Muschik, P. Schindler, D. Nigg, A. Erhard, M. Heyl, P. Hauke, M. Dalmonte, T. Monz, P. Zoller, and R. Blatt. Real-time dynamics of lattice gauge theories with a few-qubit quantum computer. *Nature*, 534(7608):516–519, June 2016.
- [27] N. Klco, E. F. Dumitrescu, A. J. McCaskey, T. D. Morris, R. C. Pooser, M. Sanz, E. Solano, P. Lougovski, and M. J. Savage. Quantum-classical computation of Schwinger model dynamics using quantum computers. *Physical Review A*, 98(3):032331, September 2018.
- [28] Alessandro Roggero and Joseph Carlson. Dynamic linear response quantum algorithm. *Phys. Rev. C*, 100:034610, Sep 2019.
- [29] Simon V. Mathis, Guglielmo Mazzola, and Ivano Tavernelli. Toward scalable simulations of lattice gauge theories on quantum computers. *Phys. Rev. D*, 102:094501, Nov 2020.
- [30] Giulia Mazzola, Simon V. Mathis, Guglielmo Mazzola, and Ivano Tavernelli. Gauge-invariant quantum circuits for  $u(1)$  and yang-mills lattice gauge theories. *Phys. Rev. Res.*, 3:043209, Dec 2021.
- [31] Sau Lan Wu, Shaojun Sun, Wen Guan, Chen Zhou, Jay Chan, Chi Lung Cheng, Tuan Pham, Yan Qian, Alex Zeng Wang, Rui Zhang, Miron Livny, Jennifer Glick, Panagiotis Kl. Barkoutsos, Stefan Woerner, Ivano Tavernelli, Federico Carminati, Alberto Di Meglio, Andy C. Y. Li, Joseph Lykken, Panagiotis Spentzouris, Samuel Yen-Chi Chen, Shinjae Yoo, and Tzu-Chieh Wei. Application of quantum machine learning using the quantum kernel algorithm on high energy physics analysis at the lhc. *Phys. Rev. Res.*, 3:033221, Sep 2021.
- [32] Giuseppe Clemente, Arianna Crippa, and Karl Jansen. Strategies for the determination of the running coupling of  $(2+1)$ -dimensional qed with quantum computing. *Phys. Rev. D*, 106:114511, Dec 2022.
- [33] Sau Lan Wu, Shaojun Sun, Wen Guan, Chen Zhou, Jay Chan, Chi Lung Cheng, Tuan Pham, Yan Qian, Alex Zeng Wang, Rui Zhang, Miron Livny, Jennifer Glick, Panagiotis Kl. Barkoutsos, Stefan Woerner, Ivano Tavernelli, Federico Carminati, Alberto Di Meglio, Andy C. Y. Li, Joseph Lykken, Panagiotis Spentzouris, Samuel Yen-Chi Chen, Shinjae Yoo, and Tzu-Chieh Wei. Application of quantum machine learning using the quantum kernel algorithm on high energy physics analysis at the lhc. *Phys. Rev. Res.*, 3:033221, Sep 2021.
- [34] Julian Schuhmacher, Laura Boggia, Vasilis Belis, Ema Puljak, Michele Grossi, Maurizio Pierini, Sofia Vallecorsa, Francesco Tacchino, Panagiotis Barkoutsos, and Ivano Tavernelli. Unravelling physics beyond the standard model with classical and quantum anomaly detection. *arXiv preprint arXiv:2301.10787*, 2023.
- [35] Kinga Anna Woźniak, Vasilis Belis, Ema Puljak, Panagiotis Barkoutsos, Günther Dissertori, Michele Grossi, Maurizio Pierini, Florentin Reiter, Ivano Tavernelli, and Sofia Vallecorsa. Quantum anomaly detection in the latent space of proton collision events at the lhc. *arXiv preprint arXiv:2301.10780*, 2023.
- [36] P. J. J. O’Malley, R. Babbush, I. D. Kivlichan, J. Romero, J. R. McClean, R. Barends, J. Kelly, P. Roushan, A. Tranter, and *et al.* Scalable quantum simulation of molecular energies. *Phys. Rev. X*, 6:031007, Jul 2016.
- [37] Abhinav Kandala, Antonio Mezzacapo, Kristan Temme, Maika Takita, Markus Brink, Jerry M Chow, and Jay M Gambetta. Hardware-efficient variational quantum eigensolver for small molecules and quantum magnets. *nature*, 549(7671):242–246, 2017.

- [38] Panagiotis Kl Barkoutsos, Jerome F. Gonthier, Igor Sokolov, Nikolaj Moll, Gian Salis, Andreas Fuhrer, Marc Ganzhorn, Daniel J. Egger, Matthias Troyer, Antonio Mezzacapo, Stefan Filipp, and Ivano Tavernelli. Quantum algorithms for electronic structure calculations: Particle-hole Hamiltonian and optimized wave-function expansions. *Physical Review A*, 98(2):1–13, 2018.
- [39] Yudong Cao, Jonathan Romero, Jonathan P Olson, Matthias Degroote, Peter D Johnson, Mária Kieferová, Ian D Kivlichan, Tim Menke, Borja Peropadre, Nicolas PD Sawaya, et al. Quantum chemistry in the age of quantum computing. *Chemical Reviews*, 119(19):10856–10915, 2019.
- [40] Sam McArdle, Suguru Endo, Alán Aspuru-Guzik, Simon C. Benjamin, and Xiao Yuan. Quantum computational chemistry. *Rev. Mod. Phys.*, 92:015003, Mar 2020.
- [41] Igor O Sokolov, Panagiotis Kl Barkoutsos, Pauline J Ollitrault, Donny Greenberg, Julia Rice, Marco Pistoia, and Ivano Tavernelli. Quantum orbital-optimized unitary coupled cluster methods in the strongly correlated regime: Can quantum algorithms outperform their classical equivalents? *The Journal of Chemical Physics*, 152(12):124107, 2020.
- [42] Pauline J Ollitrault, Abhinav Kandala, Chun-Fu Chen, Panagiotis Kl Barkoutsos, Antonio Mezzacapo, Marco Pistoia, Sarah Sheldon, Stefan Woerner, Jay M Gambetta, and Ivano Tavernelli. Quantum equation of motion for computing molecular excitation energies on a noisy quantum processor. *Physical Review Research*, 2(4):043140, 2020.
- [43] Igor O. Sokolov, Panagiotis Kl. Barkoutsos, Lukas Moeller, Philippe Suchsland, Guglielmo Mazzola, and Ivano Tavernelli. Microcanonical and finite-temperature ab initio molecular dynamics simulations on quantum computers. *Phys. Rev. Research*, 3:013125, Feb 2021.
- [44] Oriel Kiss, Francesco Tacchino, Sofia Vallecorsa, and Ivano Tavernelli. Quantum neural networks force fields generation. *Machine Learning: Science and Technology*, 3(3):035004, 2022.
- [45] Panagiotis Kl Barkoutsos, Fotios Gkritis, Pauline J Ollitrault, Igor O Sokolov, Stefan Woerner, and Ivano Tavernelli. Quantum algorithm for alchemical optimization in material design. *Chemical science*, 12(12):4345–4352, 2021.
- [46] Pauline J Ollitrault, Alexander Miessen, and Ivano Tavernelli. Molecular quantum dynamics: A quantum computing perspective. *Accounts of Chemical Research*, 54(23):4229–4238, 2021.
- [47] Max Rossmannek, Panagiotis Kl Barkoutsos, Pauline J Ollitrault, and Ivano Tavernelli. Quantum hf/dft-embedding algorithms for electronic structure calculations: Scaling up to complex molecular systems. *The Journal of Chemical Physics*, 154(11):114105, 2021.
- [48] Panagiotis Kl. Barkoutsos, Fotios Gkritis, Pauline J. Ollitrault, Igor O. Sokolov, Stefan Woerner, and Ivano Tavernelli. Quantum algorithm for alchemical optimization in material design. *Chem. Sci.*, 12:4345–4352, 2021.
- [49] Anton Robert, Panagiotis Kl Barkoutsos, Stefan Woerner, and Ivano Tavernelli. Resource-efficient quantum algorithm for protein folding. *npj Quantum Information*, 7(1):38, 2021.
- [50] Stefano Mensa, Emre Sahin, Francesco Tacchino, Panagiotis Kl Barkoutsos, and Ivano Tavernelli. Quantum machine learning framework for virtual screening in drug discovery: a prospective quantum advantage. *arXiv preprint arXiv:2204.04017*, 2022.
- [51] Alberto Baiardi, Matthias Christandl, and Markus Reiher. Quantum computing for molecular biology. *arXiv preprint arXiv:2212.12220*, 2022.
- [52] Sabrina Maniscalco, Elsi-Mari Borrelli, Daniel Cavalcanti, Caterina Foti, Adam Glos, Mark Goldsmith, Stefan Knecht, Keijo Korhonen, Joonas Malmi, Anton Nykänen, et al. Quantum network medicine: rethinking medicine with network science and quantum algorithms. *arXiv preprint arXiv:2206.12405*, 2022.
- [53] Ivan Kassal, Stephen P. Jordan, Peter J. Love, Masoud Mohseni, and Alán Aspuru-Guzik. Polynomial-time quantum algorithm for the simulation of chemical dynamics. *Proceedings of the National Academy of Sciences*, 105(48):18681–18686, 2008.
- [54] L. Veis, J. Visnak, H. Nishizawa, H. Nakai, and J. Pittner. Quantum chemistry beyond born–oppenheimer approximation on a quantum computer: A simulated phase estimation study. *Int. J. Quantum. Chem.*, 116:1328–1336, 2016.
- [55] Pauline J. Ollitrault, Guglielmo Mazzola, and Ivano Tavernelli. Nonadiabatic molecular quantum dynamics with quantum computers. *Phys. Rev. Lett.*, 125:260511, Dec 2020.
- [56] Fabijan Pavošević and Sharon Hammes-Schiffer. Multicomponent unitary coupled cluster and equation-of-motion for quantum computation. *Journal of Chemical Theory and Computation*, 17(6):3252–3258, 2021. PMID: 33945684.
- [57] Alberto Peruzzo, Jarrod McClean, Peter Shadbolt, Man-Hong Yung, Xiao-Qi Zhou, Peter J. Love, Alán Aspuru-Guzik, and Jeremy L. O’Brien. A variational eigenvalue solver on a photonic quantum processor. *Nat. Commun.*, 5:4213, 2014.
- [58] Nikolaj Moll, Panagiotis Barkoutsos, Lev S Bishop, Jerry M Chow, Andrew Cross, Daniel J Egger, Stefan Filipp, Andreas Fuhrer, Jay M Gambetta, Marc Ganzhorn, Abhinav Kandala, Antonio Mezzacapo, Peter Müller, Walter Riess, Gian Salis, John Smolin, Ivano Tavernelli, and Kristan Temme. Quantum optimization using variational algorithms on near-term quantum devices. *Quantum Sci. Technol.*, 3:030503, 2018.
- [59] Abhinav Kandala, Antonio Mezzacapo, Kristan Temme, Maika Takita, Markus Brink, Jerry M. Chow, and Jay M. Gambetta. Hardware-efficient variational quantum eigensolver for small molecules and quantum magnets. *Nature*, 249:242, 2017.
- [60] Jacob T Seeley, Martin J Richard, and Peter J Love. The bravyi-kitaev transformation for quantum computation of electronic structure. *The Journal of chemical physics*, 137(22):224109, 2012.
- [61] Sam McArdle, Suguru Endo, Alán Aspuru-Guzik, Simon C Benjamin, and Xiao Yuan. Quantum computational chemistry. *Reviews of Modern Physics*, 92(1):015003, 2020.
- [62] John Preskill. Quantum computing in the nisq era and beyond. *Quantum*, 2:79, 2018.
- [63] Jarrod R McClean, Sergio Boixo, Vadim N Smelyanskiy, Ryan Babbush, and Hartmut Neven. Barren plateaus in quantum neural network training landscapes. *Nature communications*, 9(1):1–6, 2018.

- [64] Qiskit. Qiskit: An open-source framework for quantum computing, 2021. <http://www.qiskit.org>.
- [65] Samson Wang, Enrico Fontana, Marco Cerezo, Kunal Sharma, Akira Sone, Lukasz Cincio, and Patrick J Coles. Noise-induced barren plateaus in variational quantum algorithms. *Nature communications*, 12(1):1–11, 2021.
- [66] Giuseppe M. J. Barca, Colleen Bertoni, Laura Carrington, Dipayan Datta, Nuwan De Silva, J. Emiliano Deustua, Dmitri G. Fedorov, Jeffrey R. Gour, Anastasia O. Gunina, Emilie Guidez, Taylor Harville, Stephan Irle, Joe Ivanic, Karol Kowalski, Sarom S. Leang, Hui Li, Wei Li, Jesse J. Lutz, Ilias Magoulas, Joani Mato, Vladimir Mironov, Hiroya Nakata, Buu Q. Pham, Piotr Piecuch, David Poole, Spencer R. Pruitt, Alistair P. Rendell, Luke B. Roskop, Klaus Ruedenberg, Tosaporn Sattasathuchana, Michael W. Schmidt, Jun Shen, Lyudmila Slipchenko, Masha Sosonkina, Vaibhav Sundriyal, Ananta Tiwari, Jorge L. Galvez Vallejo, Bryce Westheimer, Marta Wloch, Peng Xu, Federico Zahariev, and Mark S. Gordon. Recent developments in the general atomic and molecular electronic structure system. *The Journal of Chemical Physics*, 152(15):154102, April 2020.
- [67] Ralf Gommers, Pauli Virtanen, Evgeni Burovski, Warren Weckesser, Travis E Oliphant, David Cournapeau, Matt Haberland, Tyler Reddy, Pearu Peterson, Andrew Nelson, et al. `scipy/scipy`: Scipy 1.8.0. *Zenodo*, 2022.
- [68] Michael JD Powell. A direct search optimization method that models the objective and constraint functions by linear interpolation. In *Advances in optimization and numerical analysis*, pages 51–67. Springer, 1994.
- [69] Magnus R. Hestenes and Eduard Stiefel. Methods of conjugate gradients for solving linear systems. *Journal of Research of the National Bureau of Standards*, 49(6):409, 1952.
- [70] John L Nazareth. Conjugate gradient method. *Wiley Interdisciplinary Reviews: Computational Statistics*, 1(3):348–353, 2009.
- [71] Dieter Kraft. Algorithm 733: TOMP–Fortran modules for optimal control calculations. *ACM Trans. Math. Softw.*, 20(3):262–281, sep 1994.
- [72] Sergey Bravyi, Jay M. Gambetta, Antonio Mezzacapo, and Kristan Temme. Tapering off qubits to simulate fermionic hamiltonians. *arXiv:1701.08213*, 2017.
- [73] R. Ditchfield, W. J. Hehre, and J. A. Pople. Self-consistent molecular-orbital methods. ix. an extended gaussian-type basis for molecular-orbital studies of organic molecules. *The Journal of Chemical Physics*, 54(2):724–728, 1971.
- [74] Huber K.P. and Herzberg G. Molecular Spectra and Molecular Structure. IV. Constants of Diatomic Molecules. National Institute of Standards and Technology, 1979.
- [75] Tzvetelin Iordanov and Sharon Hammes-Schiffer. Vibrational analysis for the nuclear-electronic orbital method. *Journal of Chemical Physics*, 118(21):9489–9496, 2003.
- [76] A. Hurley. The computation of floating functions and their use in force constant calculations. *Journal of Computational Chemistry*, 9(1):75–79, 1988.
- [77] Masanori Tachikawa, Kento Taneda, and Kazuhide Mori. Simultaneous optimization of gtf exponents and their centers with fully variational treatment of hartree–fock molecular orbital calculation. *International Journal of Quantum Chemistry*, 75(4-5):497–510, 1999.
- [78] Hiromi Nakai, Keitaro Sodeyama, and Minoru Hoshino. Non-Born–Oppenheimer theory for simultaneous determination of vibrational and electronic excited states: ab initio NO+MO/CIS theory. *Chemical Physics Letters*, 345(1):118–124, 2001.
- [79] Hiromi Nakai, Minoru Hoshino, Kaito Miyamoto, and Shiaki Hyodo. Elimination of translational and rotational motions in nuclear orbital plus molecular orbital theory. *The Journal of Chemical Physics*, 122(16):164101, 2005.
- [80] Kurt R. Brorsen. Quantifying Multireference Character in Multicomponent Systems with Heat-Bath Configuration Interaction. *Journal of Chemical Theory and Computation*, 16(4):2379–2388, 2020.
- [81] Fabijan Pavošević, Tanner Culpitt, and Sharon Hammes-Schiffer. Multicomponent Quantum Chemistry: Integrating Electronic and Nuclear Quantum Effects via the Nuclear-Electronic Orbital Method. *Chemical Reviews*, 120(9):4222–4253, 2020.
- [82] Masanori Tachikawa and Yoshihiro Osamura. Isotope effect of hydrogen and lithium hydride molecules. Application of the dynamic extended molecular orbital method and energy component analysis. *Theoretical Chemistry Accounts*, 104(1):29–39, 2000.
- [83] W. Kolos and L. Wolniewicz. Nonadiabatic theory for diatomic molecules and its application to the hydrogen molecule. *Rev. Mod. Phys.*, 35:473–483, Jul 1963.
- [84] Andrea Muolo, Edit Mátyus, and Markus Reiher.  $H_3^+$  as a five-body problem described with explicitly correlated Gaussian basis sets. *Journal of Chemical Physics*, 151(15), 2019.
- [85] Yimin Wang, Bastiaan J. Braams, Joel M. Bowman, Stuart Carter, and David P. Tew. Full-dimensional quantum calculations of ground-state tunneling splitting of malonaldehyde using an accurate ab initio potential energy surface. *The Journal of Chemical Physics*, 128(22):224314, 2008.
- [86] Nanna H. List, Adrian L. Dempwolff, Andreas Dreuw, Patrick Norman, and Todd J. Martínez. Probing competing relaxation pathways in malonaldehyde with transient x-ray absorption spectroscopy. *Chem. Sci.*, 11:4180–4193, 2020.
- [87] Steven L. Baughcum, Richard W. Duerst, Walter F. Rowe, Zuzana Smith, and E. Bright Wilson. Microwave Spectroscopic Study of Malonaldehyde (3-Hydroxy-2-propenal). 2. Structure, Dipole Moment, and Tunneling. *Journal of the American Chemical Society*, 103(21):6296–6303, 1981.
- [88] Eugene M. Fluder and Jose R. De La Vega. Intramolecular hydrogen tunneling in malonaldehyde. *J. Am. Chem. Soc.*, 100(17):5265–5267, 1977.
- [89] Chr. Møller and M. S. Plesset. Note on an approximation treatment for many-electron systems. *Physical Review*, 46(7):618–622, 1934.
- [90] Yang Yang, Patrick E. Schneider, Tanner Culpitt, Fabijan Pavošević, and Sharon Hammes-Schiffer. Molecular Vibrational Frequencies within the Nuclear-Electronic Orbital Framework. *Journal of Physical Chemistry Letters*, 10(6):1167–1172,

2019.

- [91] Zachary B Charles, Miriam Farber, Charles R Johnson, and Lee Kennedy-Shaffer. The relation between the diagonal entries and the eigenvalues of a symmetric matrix, based upon the sign pattern of its off-diagonal entries. *Linear Algebra and its Applications*, 438:1427–1445, 2013.
- [92] Legeza Ö., Gebhard F., and Rissler J. Entanglement production by independent quantum channels. *Phys. Rev. B*, 74:195112, 2006.
- [93] Katharina Boguslawski, Pawel Tecmer, Örs Legeza, and Markus Reiher. Entanglement measures for single- and multireference correlation effects. *J. Phys. Chem. Lett.*, 3:3129–3135, 2012.
- [94] Katharina Boguslawski and Pawel Tecmer. Orbital entanglement in quantum chemistry. *Int. J. Quantum Chem.*, 115:1289–1295, 2015.